Finding counterparts for All-sky X-ray surveys with Nway: a Bayesian algorithm for cross-matching multiple catalogues

Mara Salvato,[1,2]* J. Buchner,[3] T. Budavári,[4] T. Dwelly,[1] A. Merloni,[1,2]
M. Brusa,[5,6] A. Rau,[1] S. Fotopoulou[7] and K. Nandra[1,8]

[1] *MPE, Giessenbachstrasse 1, Garching D-85748*
[2] *Cluster of Excellence, Boltzmann Strasse 2, D-85748*
[3] *Pontifical Catholic University of Chile, Av. Liberador Bernardo O'Higgins 328, Santiago, Región Metropolitana,Chile*
[4] *The Johns Hopkins University, 3400 N. Charles Street, Baltimore, MD 21218*
[5] *Dipartimento di Fisica e Astronomia, Universitá di Bologna, Via Gobetti 93/2, 40129 Bologna, Italy*
[6] *INAF- Osservatorio Astronomico di Bologna, Via Gobetti 93/3, 40129 Bologna, Italy*
[7] *Department of Astronomy at the University of Geneva, Chemin d'Ecogia 16, 1290 Versoix, Switzerland*
[8] *Imperial college, London, UK*

ABSTRACT

We release the AllWISE counterparts and *Gaia* matches to 106573 and 17665 X-ray sources detected in the ROSAT 2RXS and XMMSL2 surveys with |b|>15. These are the brightest X-ray sources in the sky, but their position uncertainties and the sparse multi-wavelength coverage until now rendered the identification of their counterparts a demanding task with uncertain results. New all-sky multi- wavelength surveys of sufficient depth, like AllWISE and *Gaia*, and a new Bayesian statistics based algorithm, Nway , allow us, for the first time, to provide reliable counterparts. Nway extends previous distance-based association methods and, using one or more priors (e.g., colors, magnitudes), weights the probability that sources from two or more catalogues are simultaneously associated on the basis of their observable characteristics. Here, counterparts have been determined using a WISE color-magnitude prior. A reference sample of 4524 validated XMM and *Chandra* X-ray sources demonstrates a reliability of ∼ 94.7% (2RXS2) and 97.4% (XMMSL2). Combining our results with *Chandra*- COSMOS data, we propose a new separation between stars and AGN in the X-ray/WISE flux-magnitude plane, valid over six orders of magnitude.

We also release the Nway code, including a user manual. Nway was extensively tested with XMM-COSMOS data. Using two different sets of priors, we find an agreement of 96 % and 99 % with published Likelihood Ratio methods. Our results were achieved faster and without any follow-up visual inspection. With the advent of deep and wide area surveys in X-rays (e.g. eROSITA, Athena) and radio (ASKAP/EMU, LOFAR, APERTIF, etc.) Nway will provide a powerful and reliable counterpart identification tool.

Key words: Methods: data analysis–Methods: statistical, Catalogues, X-ray Surveys, Virtual observatory tools

1 INTRODUCTION

Active Galactic Nuclei (AGN) play an important role in the evolution of galaxies in the Universe. It is now established that most massive galaxies host a supermassive black hole in their centre, and that the black hole accretion activity and history might have a profound influence on their growth. A comprehensive picture of this link can only be obtained from a complete census of AGN, covering the full luminosity function at any redshift. This is possible solely by merging AGN samples selected at different wavelengths and through complementary criteria (Padovani et al. in prep), and by combin-

---

* E-mail: mara@mpe.mpg.de (MS)

ing shallow wide-area with deep pencil beam surveys. The broad wavelength coverage is required to identify AGN at all redshifts at the wavelengths where they dominate the Spectral Energy Distribution (SED) of the galaxy (e.g., Gamma-ray: Armstrong et al. (2015); X-ray: Georgakakis & Nandra (2011); optical: Bovy et al. (2011); Palanque-Delabrouille et al. (2016); Mid-Infrared: Assef et al. (2013); Radio: De Breuck et al. (2002)). Pencil beam surveys (e.g., Luo et al. 2017) allow the study of the high-redshift population and the faint end of the luminosity distribution, while shallower wide-area surveys (e.g., Georgakakis et al. 2017; LaMassa et al. 2016) trace the brightest sources and at the same time provide access to rare objects.

The selection of AGN at X-ray energies provides an excellent compromise between completeness and purity of the sample. X-rays are sensitive to all but the most obscured AGN even when hosted in luminous galaxies, and have very low contamination from other source populations. Limited by the available datasets, and by the small field of view of the most sensitive imaging telescopes, X-ray selected AGN samples were up to now predominantly obtained from deep pencil beam surveys (e.g., COSMOS: Hasinger et al. (2007); Brusa et al. (2010); Civano et al. (2012); Marchesi et al. (2016); CDFS:Luo et al. (2010); Hsu et al. (2014); Luo et al. (2017); AEGIS-X: Nandra et al. (2015); Lockman Hole: Fotopoulou et al. (2012)) or limited to the brightest and most extreme sources (e.g., BAT: Baumgartner et al. 2013). Only very recently Stripe82X (LaMassa et al. 2016, Ananna et al., in prep) and XMM-XXL (e.g., Pierre et al. 2017; Fotopoulou et al. 2016; Georgakakis et al. 2017) opened access to two shallow, wide areas of $\approx 30\,\text{deg}^2$ and $\approx 50\,\text{deg}^2$. Still, the total population of X-ray selected known AGN counts only ≈ 20000 objects and continues to be dwarfed by the ≈ 300000 optically selected quasars (e.g., DR12Q: Pâris et al. 2017). The new revisions of the ROSAT All-sky Survey (2RXS; Boller et al. 2016) and the second release of the XMM-Newton Slew Survey (XMMSL2[1]) with a total of ≈ 130000 sources may finally provide AGN counts comparable to those found in the SDSS.

So far, the most challenging aspect of the exploitation of these samples was the identification of the multi-wavelength counterparts needed for the source characterization and redshift estimates. This was related to two shortcomings. First, the positional uncertainties of all but the brightest sources in these X-ray catalogues are in general too large to assign a single, unambiguous optical counterpart based solely on a simple coordinate match. Second, the multi-wavelengths catalogues used for identifying the counterparts lacked depth and homogeneous and contiguous coverage. At least the latter problem can now be addressed with the publicly available AllWISE survey (i.e. the combination of WISE (Wright et al. 2010) and NEOWISE (Mainzer et al. 2011, 2014)). This survey maps the entire sky at mid-infrared wavelengths from 3.4 to $22\,\mu$m to a depth at which the majority of the point- source populations of 2RXS and XMMSL2 (AGN,

stars, star-forming galaxies) is expected to be detected [2] (see § 4.1).

Even with a suitable catalogue at hand, the large X-ray positional uncertainties still require to recognize the right counterpart among the many that are possible. The most frequently used technique is based on the Likelihood Ratio (LR) method (Sutherland & Saunders 1992). Using a primary catalogue (here X-rays) and a secondary catalogue (here mid-infrared) the ratio of the likelihoods of each IR source being the true counterpart to a X-ray one or a background source is calculated taking into account the coordinates (i.e. their distances), the associated uncertainties,the density of the sources in the two catalogues and the source magnitudes and distribution. For X-ray sources with large positional uncertainties this limited set of information is often insufficient to reliably identify the counterpart. For this reason we developed a new code, Nway, that goes beyond the LR approach by simultaneously considering in addition to astrometric information (position, associated uncertainties and density of sources), various source properties (e.g. magnitudes, colors, etc.) using Bayesian statistics for each step.

In this paper, we focus on two main topics: firstly, we increase the sample of bright X-ray selected AGN by identifying and releasing the coordinates of the AllWISE counterparts to the point-like X-ray sources in 2RXS and XMMSL2 all-sky surveys. This will facilitate spectroscopic follow-up and further source characterization (see, e.g. Dwelly et al. 2017). Secondly, we present the Nway code and release it to the public, together with a detailed user manual. In order to keep the two aspects separated, the main body of the paper will only provide a short description of Nway (§ 3). Instead we will focus on the X-ray catalogues (§ 2), the construction of the prior based on AllWISE photometry (§ 4), the assessment of the reliability of our associations by comparison with literature (§ 5), and the AllWISE properties of the counterparts (§ 6), also in comparison with the results from X-ray pencil-beam surveys. The release of the catalogues is presented in § 7. The detailed description of the Nway algorithm and the verification results are made available in the Appendixes A and B. Test performances of Nway are presented in Appendix C, where we also show the strength of the method and the improvement of simultaneously using two priors instead of one.

Along the paper we assume Vega magnitudes unless differently stated. In order to allow direct comparison with existing works from the literature of X-ray surveys, we adopt a flat ΛCDM cosmology with $h = H_0/[100\text{kms}^{-1}\text{Mpc}^{-1}] = 0.7$; Ω_M=0.3; Ω_M=0.7.

2   THE DATASETS

In the following we describe the properties of the 2RXS, XMMSL2, and AllWISE catalogues and their preparation.

---

[1] https://www.cosmos.esa.int/web/xmm-newton/xmmsl2-ug

[2] Note, that the detection of an AGN in the mid-infrared requires the availability of reprocessing dust, i.e. dust free AGN will be missed. Compton-Thick AGN will be missed as well.

2.1 ROSAT All-Sky Survey

The first all-sky imaging X-ray survey in the 0.1-2.4 keV bands was performed by ROSAT (Truemper 1982) between 1990 and 1991. Besides a catalogue of extended sources, two catalogues of point-like sources were published: the Bright Source Catalogue (BSC) containing the 18,816 brightest sources (Voges et al. 1999) and the Faint Source Catalogue (FSC) encompassing the 105,924 fainter objects down to a detection likelihood limit of 6.5 (Voges et al. 2000). In view of the launch of eROSITA (Merloni et al. 2012) and taking advantage of the advancement in technology, data reduction, analysis and detection algorithms of the last 25 years, the original data have recently been reprocessed by Boller et al. (2016). The newly generated catalogue (ROSAT 2RXS) for point-like X-ray sources has been released to the community[3] and includes ≈135000 sources.

When comparing with the 1RXS catalog, which combines BSC and FSC, the number of reliable sources has increased (both bright and faint) while the number of spurious detections has decreased(see Boller et al. 2016, for more details). We extract all detections which lie within the 'extragalactic' part of the sky, i.e. with $|b| > 15$ deg, and at least 6 and 3 deg away from the optical centers of the Large and Small Magellanic Clouds, respectively. After this geometric filter, we are left with 106695 2RXS X-ray detections with an estimated coverage of ≈30575.9 deg^2. Observed in projection outside the crowded Galactic Plane, these sources are predominantly extragalactic. The catalogue is further cleaned by removing 122 sources without estimated positional uncertainty and without listed counts. The well known correlation between X-ray flux[4] intensity, positional uncertainty and detection likelihood is shown for the final 106573 sources in the primary catalogue in the left panel of Fig. 1, with the flux distribution (converted to the 0.5-2 keV band) shown in Fig. 2. 95 % of the sources have a 1σ positional error smaller than $29''$ compared to the $34''$ found in 1RXS.

2.2 *XMM-Newton* Slew 2 survey

The *XMM-Newton* European Photon Imaging Camera pn (EPIC-pn) accumulates data during slews between pointed observations. The most recent catalogue derived from this dataset covers 84 % of the sky (release 2.0, 14th March 2017). We extract all detections from the 'Clean' version of the catalogue (which we will henceforth refer to as the XMMSL2 catalogue), which lie in the same area defined for 2RXS. After this geometric filter, we are left with 22,306 X-ray detections with at least 0.1 s of effective XMMSL2 exposure with an estimated coverage of ≈25 500 deg^2.

The final catalogue was filtered to remove candidate duplicate detections of identical X-ray sources using the original column UNIQUE_SRCNAME, retaining a total of 17672 sources with 2704 sources detected only at 0.2-12 keV, 553 detected only at 0.2-2 keV and 168 sources detected only at 2-12 keV.

52.8 % (9333) of the XMMSL2 sources have at least one 2RXS source within a radius of $60''$, with 236/21/3/1/1 XMMSL2 sources being associated with 2/3/4/5/6 2RXS sources, respectively. The distribution of the positional uncertainties as a function of the flux in the detection band, color coded by the likelihood of the detection, is presented in the right panel of Fig. 1. Note, that figure shows the original positional uncertainty augmented by $5''$ in quadrature to account for the systematic uncertainty on attitude reconstruction. The flux distribution (converted to the 0.5-2 keV band) shown in Fig. 2.

2.3 AllWISE catalog

The Wide-field Infrared Survey Explorer (WISE[5]; Wright et al. 2010), was launched in 2009 and over the course of one year scanned the entire sky at least twice in the 3.4 and 4.6 μm bands (hereafter W1, W2, respectively) and at least once in the 12 and 22 μm bands (W3, W4). In the AllWISE data release[6] (November 13, 2013 Cutri et al. 2013) all the available data are combined, reaching a 5σ limiting W1, W2, W3, and W4 magnitudes of better than 17.6, 16.1, 11.5, and 7.9 (all in the Vega system) over 95 % of the extragalactic sky ($|b| > 15$ deg). The coverage is inhomogeneous, being deepest at the Ecliptic Poles.

We generated two independent catalogues that include all AllWISE sources located within a radius of $120''$ from an X-ray position listed in the 2RXS and XMMSL2 catalogues, respectively. From each catalogues duplicated sources where removed. No additional filtering was performed. This procedure results in two independent catalogues of 6,252,516 unique entries for 2RXS and 1,288,533 for XMMSL2, covering total unique areas of 368.81 deg^2 60.79 deg^2, respectively.

3 Nway IN A NUTSHELL

NWAY has been developed for identifying the multiwavelength counterparts to X-ray sources to multiple catalogues in a multi-dimensional parameter space (e.g., position, error on position, density of sources, magnitudes, colors, variability, morphology, etc.), in a Bayesian framework. The code builds on the original work of (Budavári & Szalay 2008) who developed the algorithm for matching multiple catalogues at the same time and enhances it by allowing sources to be present only in a subset of the catalogues (e.g., Pineau et al. 2017). Additionally, NWAY can either generate an internal prior for each source parameter following the implementation of the Maximum Likelihood Ratio as presented in Brusa et al. (e.g., 2007), or use an external, pre-constructed prior.

NWAY has already been successfully applied in a number of studies, e.g., the identification of counterparts to ROSAT (1RXS; Voges et al. 1999, 2000) sources in the pilot SDSS-III/SEQUELS program (P.I.: A. Merloni, P. Green Dwelly et al. 2017) using two optical bands, simultaneously; the search for counterparts to Chandra and XMM detections in the Extended Chandra Deep Field South (Hsu et al. 2014)

---

[3] http://www.mpe.mpg.de/ROSAT/2RXS
[4] We computed Galactic foreground absorption correct fluxes following the procedure presented in Appendix A of Dwelly et al. (2017)

[5] see also http://irsa.ipac.caltech.edu/Missions/wise.html for a summary and details and on the reactivated mission
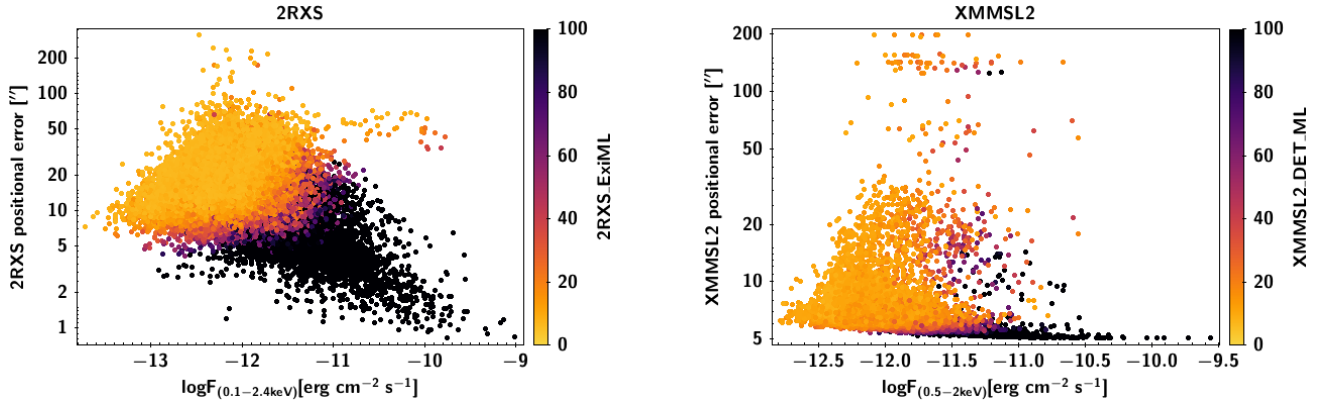[6] Available at http://wise2.ipac.caltech.edu/docs/release/allwise/

Figure 1. Positional uncertainties for the 2RXS (left) and XMMSL2 (right) samples as a function of X-ray flux. The flux of the XMMSL2 sources in the 0.2-12 keV band has been converted to the 0.5-2 keV band assuming Galactic N_H =3e20 cm^{-2} and a power-law of 1.7. For the 802 sources missing the flux in at 0.2-12 keV we converted either the flux in the 0.2-2 keV band (775 sources) or the flux in the (2-12 keV) band (27 sources). The detection likelihood reflects this procedure.
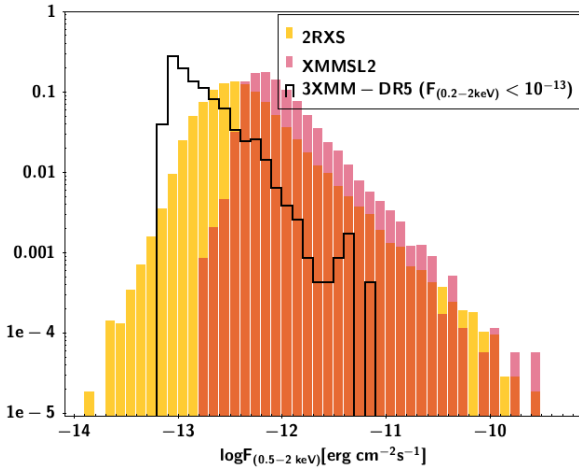

Figure 2. Flux distribution for the 2RXS (yellow), XMMSL2 (brown) and 3XMM-DR5 catalogues . The flux from the original bands has been transformed to the flux at (0.5-2 keV), assuming a Galactic N_H =3(2.29)e20 cm^{-2} and a power-law of 1.7(2.4) for XMM(ROSAT) data, respectively.

using three independent catalogues (optical, near-infrared and 3.6 μm) run simultaneously and with internally constructed priors (see for all the options the NWAY manual). It has also been applied to 1RXS and earlier XMM-Slew Survey (release 1.6, 26th Feb 2014) data on the BOSS imaging footprint (Dwelly et al. 2017), adopting an external, mid-infrared based color-magnitude prior, similar to the one adopted in this work.

A comprehensive description of NWAY is given in Appendix B together with a verification using internally generated priors for XMM-COSMOS (see Appendix C). In the following we focus on the application of the code to the scientific aim of the paper, the AllWISE counterparts to 2RXS and XMMSL2.

The NWAY code answers the question: *"Considering the astrometric information (i.e. distance from the X-ray source, positional uncertainties, and number densities) and priors (e.g. magnitude and color distribution), what is the posterior probability for each AllWISE source within a given ra-*

dius from a 2RXS or XMMSL2 detection to be the correct counterpart to the X-ray source?". For the analytical details the reader is referred to Appendix B5. In short, NWAY first computes for each source in the AllWISE catalogue the Bayes factor from the astrometric information alone. Next, the Bayes factor is weighted by the mid-infrared magnitude-color information (see § 4). Then, each AllWISE source is associated with the probability p_i of being the right counterpart to a specific X-ray detection. In addition *for each X-ray detection*, NWAY provides the probability, p_any, that the right counterpart is among the AllWISE sources. The higher the value of p_any the lower is the probability that the association is with an AllWISE source in the field. In the output catalogue of NWAY , for a given X-ray source, all the AllWISE within the search area are listed, ranked in decreasing order by their p_i. For comfort NWAY flags the first AllWISE source of each group as match_flag=1, this being the best counterpart among the available. A match_flag=2 indicates the AllWISE sources with a p_i/p_i$_{best}$ < α from the first, α being fixed by the user (in this paper it is fixed to 0.5); these are considered secondary possible counterparts. Everything else is flagged as match_flag=0.

4   APPLICATION OF NWAY TO 2RXS AND XMMSL2

In this section we motivate the AllWISE color-magnitude prior, subsequently present the results of the application of NWAY to the 2RXS and XMMSL2 catalogue defined in § 2 and finish with the comparison of the associations for sources that are in common to both X-ray catalogues .

4.1   AllWISE color-magnitude prior

The counterpart prior is defined as the probability, given observable information alone i.e. before considering any positional information, that a counterpart is related to an X-ray source. Given that the X-ray point-source population is a ensemble made of stars, nearby galaxies, and galaxies at unknown redshift hosting an AGN of unknown power, a prior based on a single magnitude distribution is insufficient. This

is especially true for X-ray detections with large positional uncertainties. Ideally, the prior would use the entire SED as discriminator (e.g. Roseboom et al. 2009). In practice, the lack of sufficiently deep multi-wavelength coverage of the entire sky requires a compromise.

The AllWISE catalogue provides photometric coverage of the entire sky in the mid-infrared, a regime where the number density of sources is low compared to e.g., the optical bands. At the same time, virtually all point-like X-ray sources found in 2RXS and XMMSL2 are expected to be detected at the depth of the AllWISE survey, as we show later in this section.

To generate the prior we need to start with an X-ray sample that matches the sources expected at the depths of 2RXS and XMMSL2 but with secure counterpart association. Beyond a comparable flux limit this sample also needs to cover a sufficiently large area to include rare and bright objects. Both characteristics are fulfilled by the 3XMM-DR5 (Rosen et al. 2016) with a sky coverage of 877 square degrees and with a flux limit significantly deeper than 2RXS and XMMSL2. Following the same screening procedure outlined in Dwelly et al. (2017), we retained 2349 sources distributed as in Fig. 2. All 2349 sources selected in this way have a unique AllWISE counterpart within $5''$, 98 % of which are within $3''$. Given the PSF of AllWISE, this provides a high confidence that the counterpart association is reliable.

The color-magnitude distribution of the AllWISE counterparts to the 3XMM-DR5 sources is shown in Fig. 3 together with the properties of the AllWISE field population. The 3XMM-DR5 counterparts are well separated from the bulk of the AllWISE population, suggesting this color-magnitude distribution to be an efficient prior. As in Dwelly et al. (2017), we generated a grid on the ([W2][W1- W2]) plane with steps of 0.25 mag in [W2] and 0.1 mag in [W1-W2] (see Figure 4) and for each bin computed the ratio of the densities of 3XMM-DR5 counterparts and field sources. This two- dimensional distribution of density ratios encodes our prior applied to the Bayes factor which was computed taking into account astrometry and sky number density of the sources.

4.2 ROSAT and AllWISE association

We have applied Nway and the prior discussed in § 4.1 to ≈ 6 Million AllWISE (see § 2.3) sources within $2'$ from the 106573 2RXS sources (see § 2.1). At least one AllWISE candidate counterpart is found for all but 93 (0.001%) 2RXS sources, with p_any histogram distribution presented with the yellow solid line in the top panel of Fig. 5.

The 93 sources without reliable AllWISE counterparts (green points in Fig. 6) are a mix bag of cases ranging from actually X-ray extended sources (e.g. 2RXS_J152238.4+083422, a spectroscopically confirmed cluster at z≈0.035) to X-ray point-like sources that a visual inspection shows on top of a very bright AllWISE object not present in the publicly released catalogue (e.g 2RXS_J150348.0+473921, 2RXS_J145123.2+190606), to sources that are very faint in AllWISE but are very bright stars in optical. Further investigation is needed for all these sources.

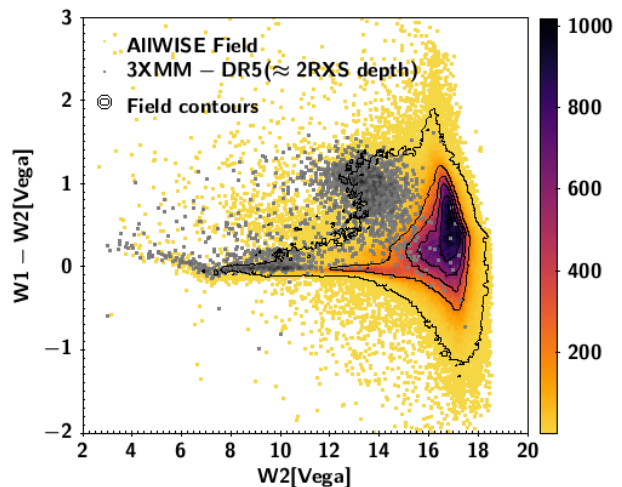63305 2RXS sources (≈59% of the sample) have p_any> 0.5 while for 35571 sources (∼33% of the sample) p_any is

Figure 3. AllWISE color-magnitude ([W1-W2] vs. [W2] distribution of counterparts to 3XMM-DR5 catalogue cut at the depth of 2RXS (grey) compared to AllWISE distribution (contours and density map) of all the sources within $2'$ from the 3XMM-DR5 sources.
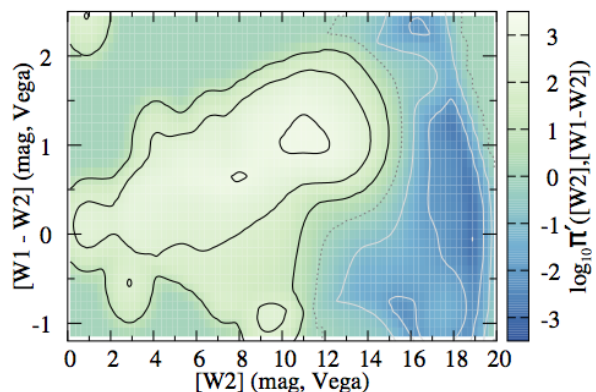

Figure 4. Map of the weighting function, π, constructed from Fig. 3 following the description in the text. Contours are drawn at $\log_{10}(\pi([W2], [W1 - W2]) = 3, 2, 1, 0, -1, -2, -3$. More description in § 4.1.

lower than 0.3. Interestingly, 60% of the latter sources have W2 magnitude fainter than 14.5. In this region the magnitude distribution of the prior overlaps with the bulk of the field population, indicating that we are at the limit of the disentangling power of the prior and that the select AllWISE counterpart could be the result of a chance association.

4.2.1 Assessing the meaning of p_any

In order to investigate what would be the typical p_any for a unreliable association, we used Nway in the same configuration, after a) shifting the coordinates of the 2RXS catalogue by $0.1°$ in Declination, b) recovering the AllWISE sources within $2'$ from the new 2RXS positions and c) removing the 2059 sources (2% of the sample) that after the shift entered in the $2'$ radius circles from the actual 2RXS sources. The distribution of p_any in this case (gold long-dashed line in the top panel of Figure 5 is peaked toward

low values of p_any, as expected, with 78%of the sample having p_any<~0.15. This coincide with the idea that in the random position of the sky there are very few sources that have the properties that match the prior. For example there are only 5% of sources that in the *randomized 2RXS sample* have p_any>0.5 and p_i > 0.8. We can easily imagine that some of these sources are counterparts to actual X-ray sources yet undetected by ROSAT, so that the association is only *marginally spurious* (i.e. it is a chance association between AllWISE and the 2RXS sources, but the sources are really X-ray emitting). These hypothesis will be validated as soon as we will have deeper X-ray data available from, e.g., eROSITA. Being very conservative, accepting as *reliable association* a p_any > 0.5 (thus with only 2% probability of chance association; see Figure 5) would result in a sample of 62944 AllWISE counterparts to 2RXS sources. However, we release here the entire catalogue of 2RXS counterparts, leaving to the user to decide the acceptable level of completeness and purity for their application. The bottom panel of Figure 5 shows the fraction of expected interlopers for any given value of p_any.

If we consider only sources with X-ray detection likelihood (EXI_ML; as defined in Boller et al. 2016) larger than 10, the fraction of sources with p_any>0.5 increase up to 80% (40207/50544). This means that many of the sources with low p_any are among those with low detection likelihood, indicating that they could be just spurious detection. The distribution of p_any for the sources with EXI_ML>10 is shown with the dotted line in Fig. 5.

4.2.2 Multiple associations

There are 17734 2RXS sources (16.6% of the entire sample) with more than one possible AllWISE counterpart [7]. Not only do most of these sources have a low p_any, but the counterparts are faint in W2 and further separated from the X-ray position, suggesting that the X-ray sources itself could be a spurious detection. Only for 7% of the 2RXS sources in this subsample p_any is larger than 0.9, with the possible counterparts located in areas well populated by the prior. Given the low resolution of ROSAT, it would be not surprising that both counterparts are actually two distinct X-ray sources, detected as one by ROSAT. The situation is well presented in the top panels of Figure 7, where we show the distribution of the AllWISE sources for the 47% (7%) of the 12321 2RXS sources with two possible counterparts having p_any<0.1 and p_any>0.9. In both panels the grey open circles represent the 3XMM-Bright sources used to build the prior, while sources in gold (green) have the higher (lower, but still comparable) p_i. The two possible associations for 2RXS_J175642.5+512108 (left) and 2RXS_J054219.4-080745 (right) are highlighted as example.

4.3 XMMSL2 and AllWISE association

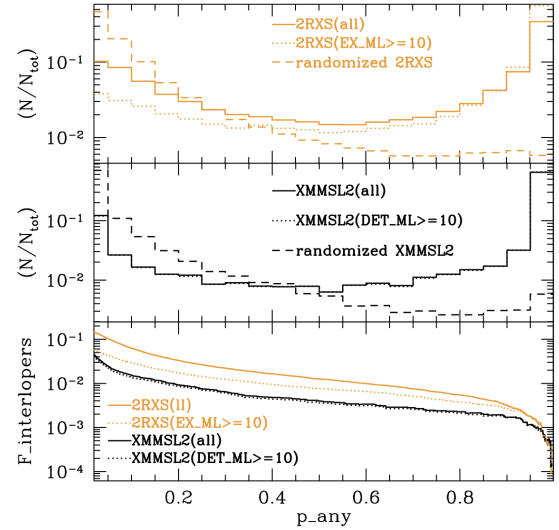The analysis done in the previous section was repeated for the XMMSL2-AllWISE association, with the summarizing

---

[7] 12321/3681/1177/386/121/34/11/2/1 cases with 2/3/4/5/6/7/8/9/10 AllWISE counterparts within the search area, respectively.

Figure 5. Histogram distribution of the probability p_any that the right counterpart is among the AllWISE sources for the 2RXS (top panel, gold) and XMMSL2 (middle panel, black) sources. The histogram is shown for the X-ray sources at the actual X-ray position (solid line) and after the randomization of the X-ray position (dashed line). The dotted lines show the distribution considering only the X-ray sources at the right position, with detection likelihood higher or equal 10. The similarity of the distribution in the case of XMMSL2 is justified by the high threshold of detection likelihood adopted in the original catalogue. The bottom panel shows at any given p_any the fraction of interlopers, measured as the fraction of sources with p_any_{random}>p_any_{real}, for the complete samples and for the samples limited at the respective detection likelihood>=10.
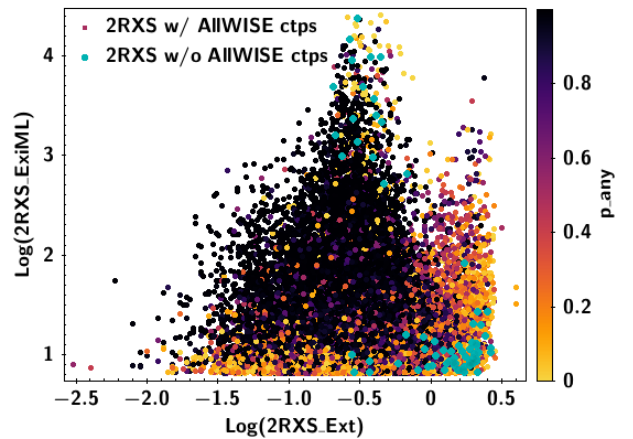

Figure 6. X-ray Extension vs. detection likelihood for the 2RXS sources, color coded as a function of p_any. Whilst sources with high p_any are widely distributed, the sources with low p_any are confined at low detection likelihood or significant extension. Green dots represent the sources for which a AllWISE counterpart was not found (see § 4.2 for more details).
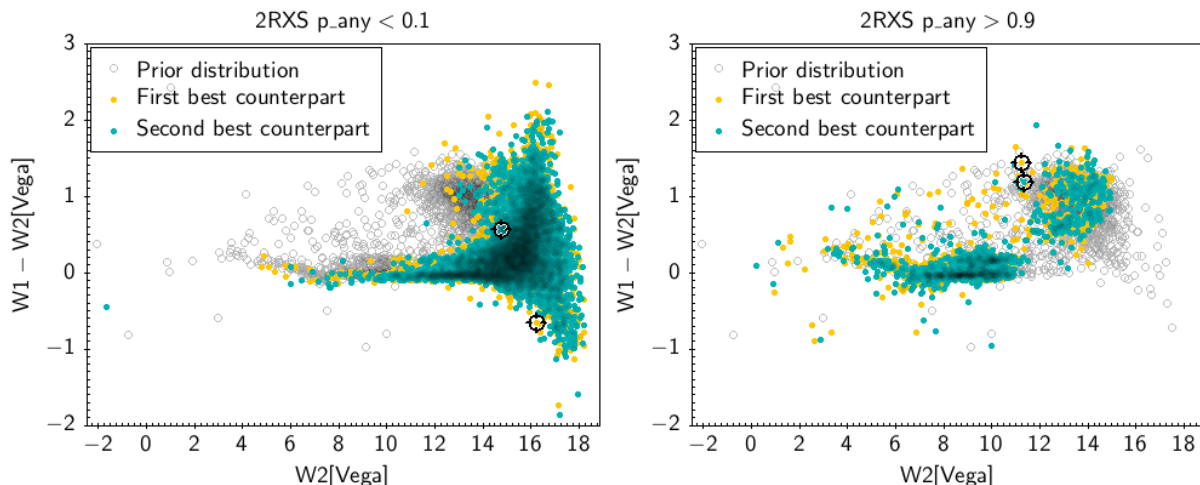
Figure 7. Primary (gold) and secondary (green) possible AllWISE counterparts to the 5844 and 899 2RXS sources having two possible counterparts and p_any<0.1 (left panel) and p_any>0.9 (right panel), respectively. The cases of 2RXS_J054219.4-080745 (left panel) and 2RXS_J175642.5+512108 (right panel) are highlighted as example. A very similar result was obtained for XMMSL2 (see text) but is not shown here for simplicity.

Table 1. XMMSL2 vs 2RXS AllWISE association for sources in common

XMMSL2-2RXS		Sources in	Identical Best
Sep.	Mean Sep.	common	AllWISE ctp.
arcsec	arcsec	N	%
≤5	3.2	1145	98.5
≤10	6.1	3559	98.5
≤30	12.4	8202	95.7
≤60	15.9	9330	91.6

plot being in the middle and bottom panels of Fig. 5. First of all, the smaller X-ray positional error of *XMM* translates into a distribution of p_any toward higher values (compare the solid and dashed cumulative curves in the right panel of the figure), with about 76% of the sources having p_any>0.5 and p_i>0.8. Only 21% of the sources have p_any<0.3 with only 8 XMMSL2 sources without any AllWISE candidate counterpart.

As for 2RXS, we randomized the positions of the XMMSL2 catalogue and run NWAY with the same setting. Now we find that for only 3% of the cases (571/17665), p_any>0.5 and p_i>0.8. The smaller positional uncertainty also reduces the fraction of sources with more than one possible counterpart. In total there are 1210 XMMSL2 sources (6.8%) with more than one possible counterpart[8]. As for 2RXS, we analyze the properties of the XMMSL2 sample with two possible counterparts. Of the 1015 sources belonging to this group, 108 (10%) have p_any>0.9 and 739 (73%) have p_any<0.3. As for 2RXS, also for XMMSL2 the majority of the sources with multiple associations have low p_any, low magnitude distribution for the possible counterpart and, above all, low detection likelihood EXI_ML_B8<10). Like for 2RXS, we will provide all the associations, leaving the user to decide on the threshold for the reliability.

---

[8] 1015/163/25/17/1/1 sources having 2/3/4/5/6/7 possible counterparts

4.4 2RXS vs. XMMSL2 associations

It is interesting to compare the association found for the sources that are in common to 2RXS and XMMSL2 as the smaller positional error of the latter catalogue can give an insight on the reliability of the association for the former one. Table 1 summarizes our results for sources that are in common within 5/10/30/60″. Overall the agreement between the associations is very good, with the higher number of identical associations happening when the two X-ray sources are closer. The little discrepancy is easily explained by the differences in the X-ray coordinates of the sources, making the search of the AllWISE counterpart within different circles.

5 COMPARISON WITH LITERATURE

Since the release of the ROSAT catalogues (Voges et al. 1999, 2000) there have been many attempts to proved the multi-wavelength counterparts to the X-ray sources. Most of the follow-up of ROSAT point-like sources concentrated on the bright sources (Rutledge et al. 2000; Schwope et al. 2000; Mahony et al. 2010), even if, with time, the methodologies adopted (association technique, secondary catalogues for the follow-up etc.) have changed. A direct comparison between those works and the ALLWISE counterparts presented in this paper is not possible as the 2RXS positions have changed from 1RXS Boller et al. (see 2016, for more details). However, it is important to bear in mind that given the low resolution of ROSAT, even if the coordinates did not change, only the availability of an X-ray survey at higher resolution than ROSAT, e.g. like eROSITA (Merloni et al. 2012) could confirm which pairing is more reliable.

It is for this reason that we decided to test our associations against a sample of 4524 validated X-ray sources from XMM and *Chandra*, in the BOSS footprint, having a reliable counterpart (see Dwelly et al. 2017, for details on the

sample). A match within $60''$ provides 1496 unique identifications in 2RXS (additional 14 2RXS sources have a second possible match). Of these, 1418 have the AllWISE counterparts coinciding with the optical counterpart, corresponding to an accuracy of 94.8%, with ≈94% of the identical associations having p_any>0.5.

The exercise repeated for XMMSL2, results in the same AllWISE counterpart for 533 of the 547 sources that have a match within $30''$ in the reference catalog, corresponding to 97.4% agreement. In 514/533 cases (96.4%) p_any>0.5 This attest both the appropriateness of the prior and the reliability of Nway .

6 SOURCES CHARACTERIZATION

For the counterparts of the 2RXS and XMMSL2 all-sky surveys there is no single survey which provides photometry and spectroscopy over the full sky. However, we can make an educated guess of the type of population by a) matching with *Gaia*[9] (Arenou et al. 2017), b) studying the AllWISE colours distribution of the counterparts and comparing them with literature (e.g., Wright et al. 2010; Nikutta et al. 2014), and, finally 3) comparing Infrared and X-ray properties of the counterparts with those well studied in the COSMOS field (XMM-COSMOS, *Chandra*-COSMOS, *Legacy Chandra*-COSMOS; Brusa et al. 2010; Civano et al. 2012; Marchesi et al. 2016, respectively).

6.1 2RXS and XMMSL2 counterparts in *Gaia*

The release of the first *Gaia* DR1 catalogue allows us to further characterize the AllWISE counterparts of 2RXS and XMMSL2. In particular, it allows us to identify those sources with a proper motion, indicating their Galactic nature. For this purpose we used the HSOY catalogue (Altmann et al. 2017) of 583'001'653 objects with precise astrometry based on the Catalogue of Positions and Proper Motions on the ICRS (PPMXL; Roeser et al. 2010) and *Gaia* DR1 (Arenou et al. 2017). We find a HSOY match within $3''$ for 91427/132216 (70%) and 14558/19120 (76%) of all the AllWISE counterparts (i.e. match_flag=1 and match_flag=2) to 2RXS and XMMSL2, respectively. Limiting the search only to the best AllWISE counterparts (i.e. match_flag=1), we obtained a match with *Gaia* for 80078/106573 (75%) and 14008/17665 (80%). Of these, 10472/80078 (13%) and 2054/14008 (15%) have a measured (above 5σ) proper motion, identifying them as stars.

6.2 IR/X-ray properties comparison with COSMOS

Originally, Maccacaro et al. (1988) noted that the AGN in the Einstein Observatory Extended Medium Sensitivity Survey (EMSS; Gioia et al. 1987) where characterized by $\log(f_x/f_V) = \pm 1$, with M stars and galaxies only marginally overlapping in this region. Since then, the locus as been adopted for the characterization of the sources practically

in all the X-ray surveys, extending the relation to other wavelength ("r", "i", "K", IRAC/[3.6 μm]) and X-ray energy bands. The validity of the locus has been always confirmed, with recent works (e.g., Brusa et al. 2007, 2010; Civano et al. 2012) pointing out that the use of the near-infrared (e.g., K band) or MIR (e.g., 3.6μm) reveals a narrower correlation than X/optical bands. Here, however, the fainter of the X-ray AGN would be below the locus (e.g., dashed line in Fig. 8 and thus overlapping more with galaxies and stars.

In this paper we extend their analysis combining the *Chandra* Legacy-COSMOS survey to 2RXS and XMMSL2. The use of *Chandra* Legacy-COSMOS survey (Civano et al. 2016; Marchesi et al. 2016) is ideal as 1) it has an homogenous depth, 2) it covers a sufficiently large area to host some bright and rare sources, 3) the counterparts are certain and well understood, thanks to the depth and amount of ancillary data available. In addition, the spectroscopic follow-up and the reliable photometric redshift via SED fitting (Marchesi et al. 2016; Salvato et al. 2011) allow the classification of the sources as Type1 (unobscured) and Type2 (obscured) AGN, Galaxies (sources with $L_X < 10^{42}$erg/s), and stars. The top panel of Fig. 8 shows the comparison between the properties of the counterparts in COSMOS and 2RXS and XMMSL2 in the [W1] vs. X-ray flux plane. The AllWISE/W1 total magnitude for the *Chandra* Legacy-COSMOS sources has been derived from the flux in IRAC/[3.6] μm within $1.9''$ aperture as listed in Laigle et al. (2016) using the conversion factor 0.765 and transforming AB to Vega magnitude as prescribed by the S-COSMOS documentation available through the Infrared Science Archive (IRAS[10]; see also Sanders et al. 2007). The additional correction of W1 - [3.6] = 0.01, following Stern et al. (2012) was applied. The COSMOS sources are also colored in magenta, green and black, indicating respectively AGN, galaxies and stars. In the same figure, when plotting the 2RXS and XMMSL2 sources, we considered for clarity only those with a detection likelihood larger than 10, p_any>0.5 and with a unique AllWISE counterpart. In the figure, the dashed line correspond to the locus define by (Maccacaro et al. 1988),

$$X/O = log(f_X/f_opt) = log(f_X) + C + mopt/2.5 = \pm 1 \quad (1)$$

but using the flux at 0.5-2 keV band and W1 magnitude, instead of the original definition of flux at 0.3-3.4 keV band and magnitude in the optical V band. The coefficient C takes into account the different effective central wavelength and width of the filter.

The solid line instead is defined as

$$[W1] = -1.625 * logF_{(0.5-2keV)} - 8.8 \quad (2)$$

with the slope corresponding to the well known relation between monochromatic X-ray and UV luminosity of unobscured, radio quiet quasars $L_X \propto L_{UV}^{0.65}$ (Lusso et al. 2010; Vignali et al. 2003; Strateva et al. 2005; Steffen et al. 2006; Just et al. 2007; Young et al. 2010), simply multiplied by -2.5 for converting luminosities to magnitudes.

The new line separates much better AGN from galaxies and stars over six orders of magnitude and passes through the bimodal distribution of the counterparts to 2RXS and XMMSL2. As for COSMOS, most of the 2RXS and XMMSL2 sources below the solid line are stars with a well measured proper motion as described in § 6.1. A complementary way to visualize this natural separation is to plot the histogram distribution of the sources with [W1] above or below the solid line, as in the bottom panel of Fig. 8. Here the stars are indicated with a solid line, while non-stars are represented with a full colored histogram. Interestingly, 98.7% of the AGN spectroscopically confirmed, presented in Dwelly et al. (2017) lie above the solid line, suggesting that most of these sources are indeed AGN. Similarly, only 0.02% of all the AllWISE counterparts to 2RXS and Such "universal" X-ray to MIR flux ratio could be explained if both UV and IR fluxes are equally good proxies of total AGN bolometric luminosity. We suggest this new empirical X-ray/MIR relation could be used as a simple mean to perform stars/quasars separation for X-ray point-like sources. In fact as we show in the next section, most of the sources below the line, despite not having a measured proper motions, are also stars, based on their AllWISE colors. Inversely, only 0.03% of the AllWISE counterparts to 2RXS and XMMSL2 that are classified as AGN using the WISE colors as defined by (Stern et al. 2012; Assef et al. 2013), lie below the solid line.

6.3 IR properties of 2RXS and XMMSL2 counterparts

The AllWISE colors [W1-W2] and [W2-W3][11] of the sources can be used for their qualitative characterization, as suggested by Wright et al. (e.g. 2010); Nikutta et al. (e.g. 2014, etc.). Fig. 9 shows the AllWISE colors of the 2RXS (left) and XMMSL2 (right) counterparts, using in background Fig. 12 of Wright et al. (2010). To the well known loci we added the location of the Fermi/Blazars identified by, e.g. D'Abrusco et al. (2013). That is also the location of most of the X-ray sources that are associated to radio emission (e.g., NVSS: Condon et al. 1998) (4308 sources in 2RXS and 1307 in XMMSL2, respectively). As suggested by Tsai et al. (2013), the sources in this locus are nearby objects (z<0.5), with jets, suggesting indeed the presence of an AGN in their cores (Emonts private communication, Emonts et al, in prep). Without any surprise, the bulk of the X-ray population in 2RXS and XMMSL2 is characterized by QSO, AGN and stars.

7 CATALOGUES RELEASE

We release the AllWISE associations to the sources in the 2RXS and XMMSL2 catalogues, outside the Galactic plane. The list and the description of columns are provided for each catalogue in the two following sections. In short, we provide few columns that are keys to the identification of
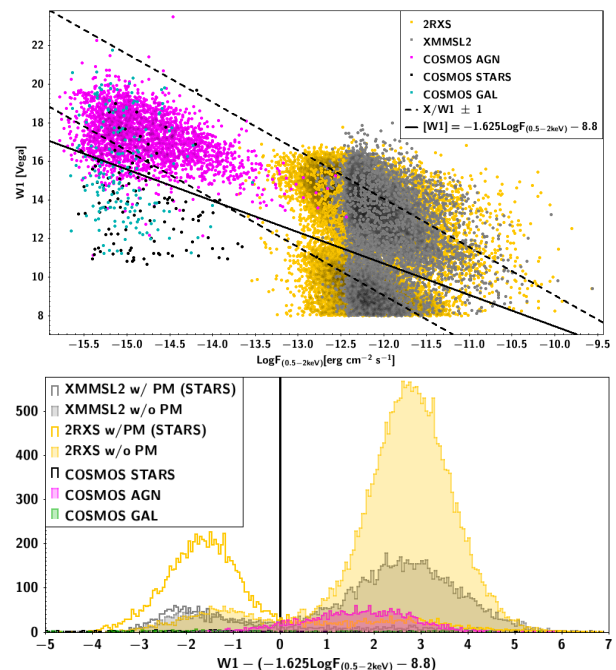
[11] 0.02% (0.08%), 0.07% (0.3%) and 20% (20%) are only upper limits in W1,W2,W3 in 2RXS (XMMSL2), respectively.

Figure 8. Top: W1 magnitude plotted against the 0.5-2 keV flux for the counterparts to *Chandra* Legacy-COSMOS survey (magenta, green, black) and for the AllWISE counterparts to 2RXS (yellow) and XMMSL2 (grey) sources with detection likelihood larger that 10 and p_any>0.5 . The COSMOS sources are colorcoded as a function of their SED (AGN, galaxies and stars) determined either via spectroscopy or via best fit of templates to their photometry. The dashed lines define the AGN locus historically defined by Maccacaro et al. (1988) and revised by Civano et al. (2012) as described in § 6.2. The solid line has the slope as defined in Eq. 2 and best separated the star/non-star bimodal distribution of the sources in the three surveys. The cuts at [W1]≈11 and [W1]=8 correspond to the saturation limits for IRAC/[3.6] μm in COSMOS and [W1] in AllWISE. **Bottom:** Histogram distribution of [W1] with respect to the solid line. Most of the sources below the line (left in this plot) are stars with a measured proper motion. Most of the sources above the line are supposed to be AGN as the distribution of the AGN in COSMOS would suggest.

the X-ray sources, simply extracted, without any modification, from their original catalogues. We complement each source with the list of possible AllWISE counterparts and the output columns of Nway that are essential for those users interested in defining more pure and complete subsamples. We provide columns that inform the user on whether or not there is more than one possible counterpart. Finally, the data are complemented with a match to the *Gaia* DR1 catalog. A simple match with the unique identifier from 2RXS, XMMSL2, AllWISE, 2MASS and *Gaia* will allow the user to retrieve additional columns from the original catalogues, not listed in our release. The catalogues will be available via Vizier and also at the dedicate web page http://www.mpe.mpg.de/XraySurveys/2RXS_XMMSL2/.

7.1 2RXS-AllWISE catalogue

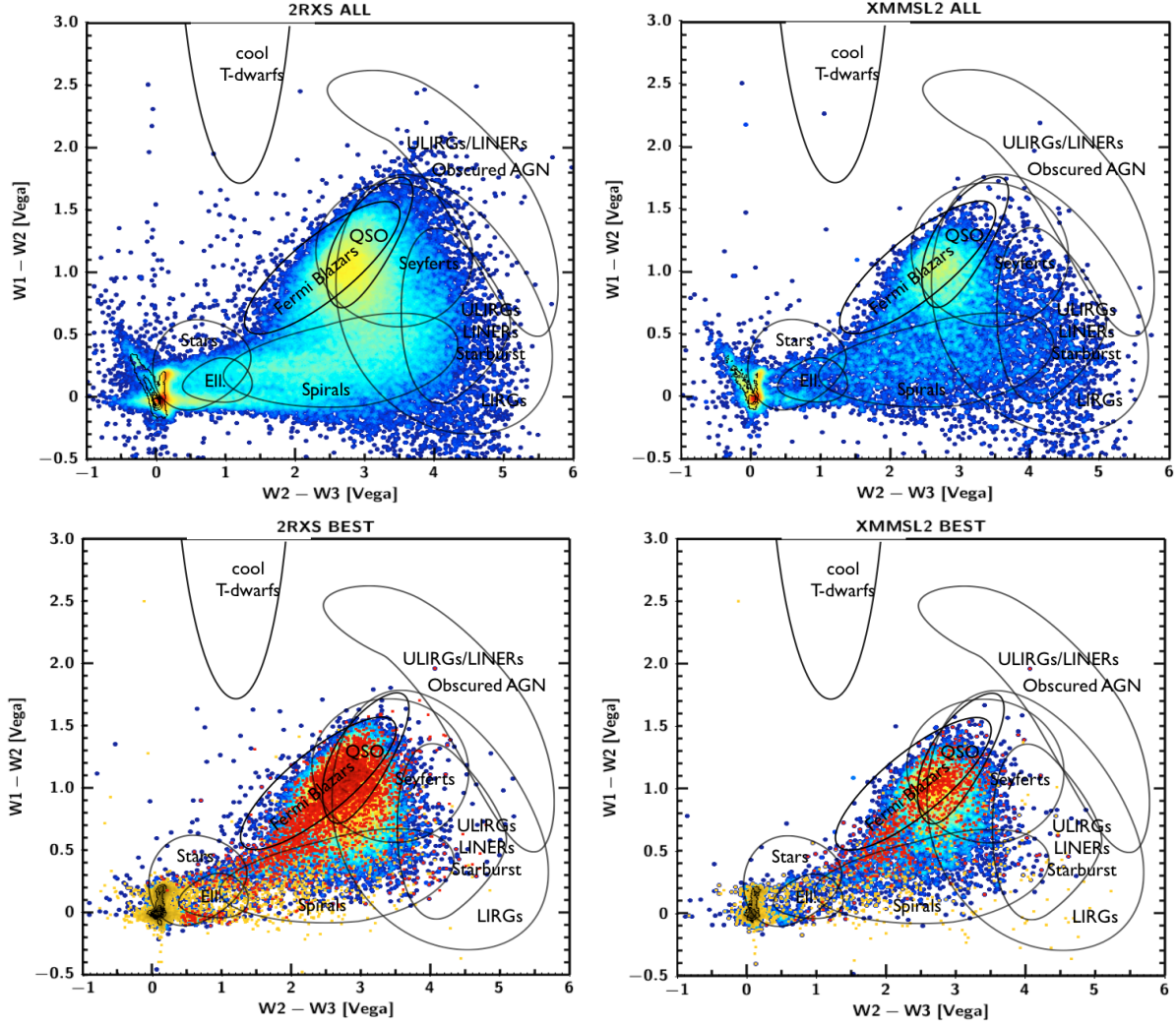*Column 1.* **2RXS_ID**: IAU Identifier from Boller et al. (2016).

Figure 9. Density distribution of the AllWISE colors of counterparts to 2RXS (Left) and XMMSL2 (Right), plotted over the color-color diagram originally created by Chao-Wei Tsai, (used here with permission) but modified by adding the approximative locus of the counterparts to Fermi sources (e.g., D'Abrusco et al. 2013). **Top:** the AllWISE counterparts are plotted for all the 2RXS and XMMSL2 sources. The contours in the (0,0) region indicated the location of the AllWISE saturated sources. **Bottom:** Only the counterparts to Xray sources with a detection likelihood larger than 10, with p_any> 0.5 and with a unique counterpart are plotted. Yellow sources on the lower-left part of the plots are stars measured proper motion. Black contours in the same area indicate the distribution of the sources that do not have a measured proper motion but are below the solid line defined in Fig. 8. The location of their concentration indicates that most of them, as expected, are stars. Red is used for indicating the sources with a NVSS counterpart, with the bulk of the distribution included within the locus of the Fermi/Blazars sources.

Columns 2-3. **2RXS_RA, 2RXS_DEC**: 2RXS J2000 Right Ascension and Declination.

Column 4. **2RXS_e_RADEC**: 2RXS positional error, in arc seconds.

Column 5 **2RXS_ExiML**: 2RXS source Detection Likelihood. User should refer to the Boller et al. (2016) for discussion on the fraction of false detections as function of this parameter.   *Column 6.* **2RXS_Ext**: 2RXS source extent in units of image pixels.

Column 7. **2RXS_ExtML**: Probability of the 2RXS source extend.

Column 8. **2RXS_SRC_FLUX**: 2RXS flux in unit of $\mathrm{erg\,cm^{-2}\,s^{-1}}$ (see Dwelly et al. 2017, for details).

Column 9. **2RXS_SRC_FLUX_ERR**: 2RXS flux error (see Dwelly et al. 2017, for details).

Column 10. **ALLW_ID**: WISE All-Sky Release Catalogue name (Cutri et al. 2013).

Columns 11-12. **ALLW_RA, ALLW_DEC** : J2000 All-WISE Right Ascension and Declination.

Column 13. **ALLW_e_RADEC**: AllWISE positional error, in arc seconds.

Columns 14-17. **ALLW_w[1234]mpro**: AllWISE Vega magnitude in the W1, W2, W3, W4 bands.

Columns 18-21. **ALLW_w[1234]sigmpro**: AllWISE magnitude error in the W1, W2, W3, W4 bands.

Columns 22-25. **ALLW_w[1234]snr**: AllWISE signal to noise ratio in the W1, W2, W3, W4 bands.   *Column 26.* **ALLW_cc_flags**: AllWISE reliability flag from Cutri et al. (2013).

Column 27. **Separation_ALLW_2RXS**: Separation be-

tween members of this association, in arcsec.

Column 28. **dist_bayesfactor**: Logarithm of ratio between prior and posterior from distance matching.

Column 29. **dist_post**: Distance posterior probability comparing this association vs. no association, as in (Budavári & Szalay 2008).

Column 30. **bias_ALLW_COLOURMAG_PIX**: Probability weighting introduced by AllWISE prior. 1 indicates no change.

Column 31. **p_single**: Same as dist_post, but weighted by the AllWISE color-magnitude prior.

Column 32. **p_any**: For each entry in the X-ray catalogue, the probability that any of the associations is the correct one. The lower p_any, lower is confidence that a reliable counterpart was found. See § 4.2.

Column 33. **p_i**: Relative probability of the match, if one exists. The p_i sum up to unity for each X-ray source.

Column 34. **match_flag**: 1 for the most probable match, if existing; 2: almost as good solutions ($p\_i/p\_i_{best} > 0.5$).

Column 35-36. **GroupID, GroupSize**: if the 2RXS source has only one possible AllWISE counterpart, the two columns are blank. Otherwise, the GroupSize value indicate the number of possible counterparts while the GroupID value is the same integer for the group. A sort on the GroupID value, will rank the first non-unique match group together, followed by all the rows in the second non-unique group, etc. All the unique matches are listed last.

Column 37. **1RXS_ID**: Source name in the 1RXS catalogues (Voges et al. 1999, 2000).

Column 38. **ALLW_2MASS_ID**: 2MASS Identifier as listed in the AllWISE catalog.

Columns 39-41. **ALLW_[jhk]_m_2mass**: 2MASS magnitude in the j,h,k bands, as from AllWISE catalogue.

Columns 42-44. **ALLW_[jhk]_msig_2mass**: 2MASS magnitude errors in the j,h,k bands, as from AllWISE catalogue.

Columns 45. **Gaia_DR1_ID**: Solution ID from the original *Gaia* DR1 catalogue (see Fabricius et al. 2016, for more details).

Columns 46-47. **Gaia_DR1_RA, Gaia_DR1_DEC**: *Gaia* J2000 Right Ascension and Declination as computed by Vizier.

Columns 48-49. **pmra, pmdec**: Proper motion in Right Ascension and Declination as measured by *Gaia*.

Columns 50-51. **pmra_error, pmdec_error**: Proper motion errors in Right Ascension and Declination as measured by *Gaia*.

Columns 52. **phot_g_mean_flux**: *Gaia* mean flux in units of e-/s.

Columns 53. **phot_g_mean_flux_error**: *Gaia* mean flux error in units of e-/s.

Columns 54. **phot_g_mean_mag**: *Gaia* mean magnitude.

7.2 XMMSL2-AllWISE catalogue

Column 1. **XMMSL2_ID**: Unique identifier from Boller et al. (2016).

Columns 2-3. **XMMSL2_RA, XMMSL2_DEC**: 2RXS J2000 Right Ascension and Declination.

Column 4. **XMMSL2_e_RADEC**: XMMSL2 original positional uncertainty augmented by $5''$ in quadrature.

Columns 5-7. **XMMSL2_DET_ML_B[876]**: XMMSL2 source Detection Likelihood in the respective energy bands.

Column 8-10. **XMMSL2_Ext_B[876]**: XMMSL2 source extent in units of image pixels, in the respective energy bands.

Column 11-13. **XMMSL2_Ext_ML_B[876]**: Probability of the XMMSL2 source extend in the respective energy bands.

Column 14-16. **XMMSL2_FLUXB[876]**: XMMSL2 flux in the respective energy bands, in $\mathrm{erg\,cm^{-2}\,s^{-1}}$ units.

Column 17-19. **2RXS_FLUX_B[876]_ERR**: XMMSL2 flux errors in the respective energy bands, in $\mathrm{erg\,cm^{-2}\,s^{-1}}$ units.

Column 20. **ALLW_ID**: WISE All-Sky Release catalogue name (Cutri et al. 2013).

Columns 21-22. **ALLW_RA, ALLW_DEC** : J2000 All-WISE Right Ascension and Declination.

Column 23. **ALLW_e_RADEC**: AllWISE positional error, in arc seconds.

Columns 24-27. **ALLW_w[1234]mpro**: AllWISE Vega magnitude in the W1, W2, W3, W4 bands.

Columns 28-31. **ALLW_w[1234]sigmpro**: AllWISE magnitude error in the W1, W2, W3, W4 bands.

Columns 32-35. **ALLW_w[1234]snr**: AllWISE signal to noise ratio in the W1, W2, W3, W4 bands. *Column 36.* **ALLW_cc_flags**: AllWISE reliability flag from Cutri et al. (2013).

Column 37. **Separation_ALLW_XMMSL2**: Separation between members of this association, in arcsec.

Column 38. **dist_bayesfactor**: Logarithm of ratio between prior and posterior from distance matching.

Column 39. **dist_post**: Distance posterior probability comparing this association vs. no association, as in (Budavári & Szalay 2008).

Column 40. **bias_ALLW_COLOURMAG_PIX**: Probability weighting introduced by AllWISE prior. 1 indicates no change.

Column 41. **p_single**: Same as dist_post, but weighted by AllWISE prior.

Column 42. **p_any**: For each entry in the X-ray catalogue, the probability that any of the associations is the correct one. The lower p_any, lower is confidence that a reliable counterpart was found. See § 4.2.

Column 43. **p_i**: Relative probability of the match, if one exists. The p_i sum up to unity for each X-ray source.

Column 44. **match_flag**: 1 for the most probable match, if existing; 2: almost as good solutions ($p\_i/p\_ibest > 0.5$).

Column 45-46. **GroupID, GroupSize**: if the 2RXS source has only one possible AllWISE counterpart, the two columns are blank. Otherwise, the GroupSize value indicate the number of possible counterparts while the GroupID value is the same integer for the group. A sort on the GroupID value, will rank the first non-unique match group together, followed by all the rows in the second non-unique group, etc. All the unique matches are listed last.

Column 47. **ALLW_2MASS_ID**: 2MASS Identifier as listed in the AllWISE catalog.

Columns 48-50. **ALLW_[jhk]_m_2mass**: 2MASS magnitude in the j,h,k bands, as from AllWISE catalogue.

Columns 51-53. **ALLW_[jhk]_msig_2mass**: 2MASS magnitude errors in the j,h,k bands, as from AllWISE catalogue.

Columns 54. **Gaia_DR1_ID**: Solution ID from the original *Gaia* DR1 catalogue (see Fabricius et al. 2016, for more

details).

Columns 55-56. **Gaia_DR1_RA, Gaia_DR1_DEC**: *Gaia* J2000 Right Ascension and Declination as computed by Vizier.

Columns 57-58. **pmra, pmdec**: Proper motion in Right Ascension and Declination as measured by *Gaia*.

Columns 59-60. **pmra_error, pmdec_error**: Proper motion errors in Right Ascension and Declination as measured by *Gaia*.

Columns 61. **phot_g_mean_flux**: *Gaia* mean flux in units of e-/s.

Columns 62. **phot_g_mean_flux_error**: *Gaia* mean flux erorr in units of e-/s.

Columns 63. **phot_g_mean_mag**: *Gaia* mean magnitude.

8 Nway RELEASE

Together with the AllWISE counterparts to the 2RXS and XMMSL2 catalogues, we release also NWAY. NWAY software and manual are available at https://github.com/JohannesBuchner/nway. In order to make the user familiar with the code, the release is completed with the catalogues used in the testing phase discussed in Appendix C. We would like to stress that the use of NWAY is not limited to finding the counterparts to X-ray sources. With the advent of deep and wide area surveys in X-rays (e.g. eROSITA, Athena) and radio (e.g., ASKAP/ EMU:Norris et al. (2011); LOFAR:van Haarlem et al. (2013); APERTIF:Oosterloo et al. (2010)) NWAY will provide a powerful and reliable counterpart identification tool.

9 DISCUSSION AND CONCLUSIONS

We have presented the catalogues of secure AllWISE counterparts to the ROSAT/2RXS and XMMSL2 X-ray extragalactic all-sky surveys, with only a marginal fraction of less than 5% of the X-ray/AllWISE associations expected to be due to chance associations. The associations were obtained by mean of a new algorithm, NWAY capable of handling complicated priors. In particular, we have used here a prior based on the WISE color-magnitude properties of about 2500 X-ray sources from the 3XMM-DR5 catalogue with flux distribution similar to 2RXS and XMMSL2.

While it is clear that NWAY can be used for finding the right counterparts to other (not only X-ray) surveys, the same can not be said for the prior adopted here because, if not appropriated, the prior can affect the results. For example, adopting for 2RXS the same prior used in Dwelly et al. (2017), which was constructed with half of the sources adopted here, the AllWISE counterpart changes for 3% of the sources (3431/106573). The prior is appropriate only as long as it well represents the population. For this reason, the prior adopted for the extragalactic region covered by 2RXS and XMMSL2 can not be used with the same reliability for finding the correct counterparts of X-ray sources in the galactic plane, dominated by stars. Similarly, it will not be possible to use the same prior with the same reliability

for finding the counterparts to X-ray surveys deeper than the two discussed in this work.

9.1 Finding the counterparts to the eROSITA point-like sources

The design and development of NWAY was dictated by the need of having a flexible algorithm that could be used with the patchwork of multi-wavelength coverage of the All-Sky available for finding the counterparts of eROSITA (Merloni et al. 2012).

eROSITA combines a wide field of view, large collecting area, long survey duration, broad energy bandpass, and good point source location accuracy, making it by far the most powerful X-ray survey instrument ever built. In the soft energy band (0.5–2 keV), the planned four-year eROSITA all-sky survey, will have a median point source flux limit of $10^{-14}\,\mathrm{erg\,cm^{-2}\,s^{-1}}$ (Merloni et al. 2012), approximately a factor of $30\times$ deeper than ROSAT all-sky survey (for AGN-like X-ray spectra).

In the hard X-ray band (2–10 keV), the predicted flux limit of $2 \times 10^{-13}\,\mathrm{erg\,cm^{-2}\,s^{-1}}$ is around 100 times deeper than the only existing all-sky survey conducted at these energies (i.e. the High Energy Astronomy Observatory, HEAO-I: Wood et al. 1984)). On completion, the eROSITA survey is expected to detect about 4 millions X-ray sources, with 3/4 of them being AGN in the extragalactic sky.

Thankfully, the location accuracy for point-like eROSITA sources is expected to be better than $10''$ radius (combination of statistical and systematic uncertainties), substantially better than for typical ROSAT sources. This will be also enabled by the availability of *Gaia* that will allow accurate positional accuracy on eROSITA single frame by tying the two astrometric reference frames. The eROSITA data will also enable better separation between point-like (mostly AGN and stars) and extended (galaxy cluster) sources on the basis of their X-ray properties alone (Merloni et al. 2012). However, due to the fainter X-ray flux limit expected, the optical-IR counterparts to point-like eROSITA sources will typically be several magnitudes fainter than those presented here. Figure 10 illustrates the point. The figure shows a sample of ~ 4500 XMM and *Chandra* validate sources as a proxy for eROSITA at its all-sky depth, at the end of the mission. Given the increasing depth of eROSITA, the counterparts of the sources get progressively fainter, finally overlapping with the bulk of the All-WISE population, here in grey (see for comparison the distribution in Fig. 3).

Hence, in order to select the correct counterparts for the millions of eROSITA sources, we will need to take into account additional information to separate field populations from the true counterparts to X-ray sources. Deeper WISE catalogues, enabled by the co-addition of the ongoing multi-year NEOWISE survey data (Mainzer et al. 2011, 2014; Meisner et al. 2016) with the existing AllWISE data set, should not only probe to fainter $[W1]$ and $[W2]$ limits, but should also have a smaller photometric scatter at the magnitudes currently probed by the AllWISE survey. Such a reduced scatter will allow better separation of the red (in $[W1\text{-}W2]$) AGN population from the bluer field stars and galaxies. Note however that at the depth of ROSAT, only 0.01% of the AllWISE counterparts had an upper limit in

W2, while the number will increase at fainter X-ray flux, even considering the reactivation of NEOWISE (Mainzer et al. 2014; Meisner et al. 2017) post-cryogenic phase expected to reach a depth in W2 of 19.9, when combined with WISE.

In addition, we expect that one of the main drawbacks of relying on any catalogue derived from WISE data will be the relatively broad PSF (∼6 arcsec full width at half maximum in WISE bands 1 and 2), which results in blending problems for close pairs of sources. This problem will inevitably get worse as the co-added WISE data reaches to fainter magnitudes, approaching the confusion limit. In addition, once an AllWISE counterpart has been selected for each X-ray source, the final step of optical counterpart selection must still be carried out. This step becomes particularly difficult when WISE detections are blends of multiple astrophysical sources.

The forced photometry techniques and tools described by Lang et al. (2016) avoid many of the problems associated with combining data across multiple wavebands, and have already been exploited successfully e.g. in the selection of QSO targets for eBOSS (Myers et al. 2015). By crossmatching eROSITA sources with previously compiled forced photometry catalogue (e.g. derived from *Gaia* in the Galactic plane, SDSS and DECaLS, DES, VHS photometry), we expect to greatly reduce both the impact of source confusion in the IR, and the general problems related to compiling data across multiple optical-IR wavebands.

The high cross-matching success rate for 2RXS and XMMSL2 has demonstrated that our cross-matching routine and priors are relatively robust. However, the dynamic range of the eROSITA catalogue will be much larger than that considered here.

Therefore, it is likely that a single, X-ray fluxindependent prior (as adopted in this work) will be a suboptimal choice for finding counterparts to *all* eROSITA sources. We also expect a strong dependence in the mixture of object classes which make up the eROSITA sample as a function of Galactic latitude. Thankfully, the XMM, Chandra and SWIFT-XRT archives already contain large samples of well-measured X-ray reference sources which populate the entire eROSITA flux range, and which can be used to define new X-ray-flux-dependent and/or Galactic-latitudedependent optical-IR priors.

However, great care will be needed to understand the very complex inhomogeneities/biases/incompletenesses that will be imprinted by such an optimized cross-matching scheme. It is possible that a single cross-matching procedure is not suitable for all eROSITA science projects, and that a number of individually tailored cross-matching schemes will be required, depending on the patch on the sky.

The bulk of the X-ray sources in our study are stars and AGN, which are intrinsically variable objects. However, we have made the simplifying assumption throughout this work that variability (in luminosity and/or in spectral energy distribution) of X-ray sources is not important for the purposes of counterpart selection. This means that we do not take account of extremely interesting, but difficult to handle scenarios such as where an AGN that was bright at the epoch of its X-ray detection (e.g. in ROSAT) has faded substantially (in all wavebands) several years later when the measurement of its longer wavelength counterpart (e.g. WISE
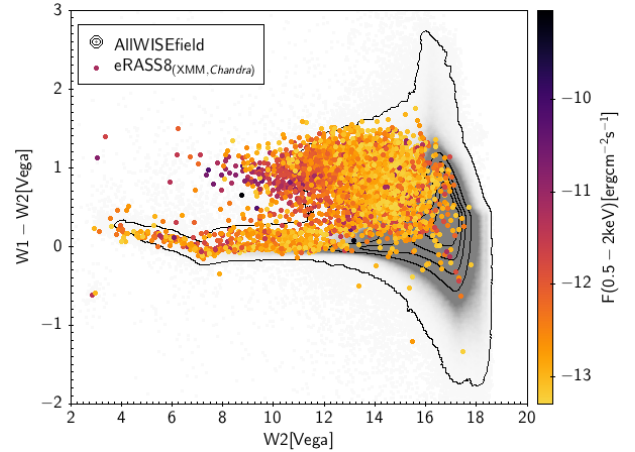
Figure 10. WISE color-magnitude plane for the AllWISE counterparts to the X-ray validated sample used in § 5, cut at the expected depth of eROSITA at the end of the survey (eRASS:8). Sources are color coded as a function of their X-ray flux. In grey the AllWISE population is shown. As the depth of eROSITA increases, the AllWISE counterparts will overlap with the bulk of the AllWISE population, thus reducing the disentangling power of the prior.

or SDSS) was made (e.g. 'changing-look' QSOs; LaMassa et al. 2015; Merloni et al. 2015; Runnoe et al. 2016). However, in the future we will use AGN and stellar variability to our advantage when selecting counterparts to eROSITA X-ray sources. With the present (PTF/iPTF/ZTF[12]Rau et al. (2009); Catalina [13], Pan-STARRS[14]: Chambers et al. (2016); etc.) and forthcoming generation of optical time domain surveys, (e.g. as performed by the Large Synoptic Survey Telescope; Gressler et al. 2014), every potential optical counterpart to an X-ray source will also come with robust measurements of optical variability. Such variability metrics, which naturally separate AGN and stars from field galaxies, and can be simply applied as an additional prior in Nway (see, for example, Budavári et al. 2017).

---

[12] http://www.ptf.caltech.edu/iptf
[13] http://crts.caltech.edu/
[14] https://panstarrs.stsci.edu/

compiled by the 10 institutes of the XMM-Newton Survey Science Centre selected by ESA. This publication makes use of data products from the Two Micron All Sky Survey, which is a joint project of the University of Massachusetts and the Infrared Processing and Analysis Center/California Institute of Technology, funded by the National Aeronautics and Space Administration and the National Science Foundation. This research has made use of data obtained from XMMSL2, the Second XMM-Newton Slew Survey Catalogue, produced by members of the XMM SOC, the EPIC consortium, and using work carried out in the context of the EXTraS project ("Exploring the X-ray Transient and variable Sky", funded from the EU's Seventh Framework Programme under grant agreement no. 607452). This work has made use of data from the European Space Agency (ESA) mission *Gaia* (https://www.cosmos.esa.int/gaia), processed by the *Gaia* Data Processing and Analysis Consortium (DPAC, https://www.cosmos.esa.int/web/gaia/dpac/consortium). Funding for the DPAC has been provided by national institutions, in particular the institutions participating in the *Gaia* Multilateral Agreement. This research has made use of the Vizier catalogue access tool, CDS, Strasbourg, France. The original description of the VizieR service was published in A&AS 143, 23. This publication makes use of TOPCAT (Taylor 2005) and STILTS (Taylor 2006) available at http://www.starlink.ac.uk/topcat/ and http://www.starlink.ac.uk/stilts/, respectively.

APPENDIX A: A BRIEF HISTORY OF THE MATCHING PROBLEM

In astrophysics a source can be characterized by its accurate position on the sky, its redshift and its Spectral Energy Distribution (SED). If the positional accuracy is not known at a sub-arc second precision, the source can not be the target of a spectroscopy study, and/or multi wavelength data can not be correctly assembled. While sources that are identified in the Optical and Near-Infrared regime usually have the required precision, this is not the case for sources selected at shorter and longer wavelengths. For example in the Far-infrared bands, Herschel reaches 6-7″ Point Spread Function (PSF) at 70μm, increasing up to ∼13″ at longer wavelength. Similarly, in X-ray the positional measurement error depends on the counts and spatially varying PSF and therefore is not constant between sources. Typical values go from up to ≈ 3″ (*Chandra*), to 7″ (*XMM*) but reach up to about 29″ for 95% of the of ROSAT sources in 2RXS, with the values increasing toward the periphery of the field of view, up to more than 1′ in the extreme cases. This low resolution, together with the fact that sources with different SEDs and different redshift emit the bulk of their energy in different photometric bands, make it difficult to identifying with certainty the *same* source in different surveys. Additionally, the entire pairing process is done by means of catalogues which can differ in depth, technique for "source detection" (and definition thereof). In the past, the data were so shallow that a simple cross match in coordinates between catalogues was enough for pairing correctly the sources. Now, we reach sources that are so faint that we must adopt a probabilistic approach.

The most used technique is based on the Likelihood

Ratio (LR) method (Sutherland & Saunders 1992). Taking into account source number densities, coordinates (with relative errors) and magnitude distribution of the sources, the method estimates the ratio between the likelihood that a given source from catalogue B is the correct counterpart to a source detected in a catalogue A, and the likelihood of being a source in the background. Different factors are then considered when computing the threshold above which the likelihood ratio assures a reliable association. The procedure is repeated anew for the pairing between the catalogues A-C, A-D, etc. If catalogues are i)from images at similar wavelength and ii)of sufficient depth, for most of the sources in A, the counterpart in catalogues B, C, D etc will be the same, while for a fraction of the sources further considerations based on the shape of the SED need to be taken into account for the counterpart association.

Moving from a generic description to a specific application, let us focus from now on to the case of finding the correct counterpart to X-ray sources. The LR method has been successfully applied on surveys like XMM-COSMOS (Brusa et al. 2007, 2010), CDFS (Luo et al. 2008; Xue et al. 2011; Luo et al. 2017), *Chandra*-COSMOS (Civano et al. 2012; Marchesi et al. 2016), XXL (Georgakakis et al. 2017), STRIPE-82X (LaMassa et al. 2016, Ananna et al., in prep), AEGIS-X (Georgakakis & Nandra 2011; Nandra et al. 2015) just to mention a few. For each of these surveys, the authors have performed the steps described above, pairing X-ray to Optical, to near Infrared and to Mid-infrared data, independently. Then, they ranked the ancillary data available in order of reliability (i.e. deep and higher resolution data first) for selecting the correct counterpart in those cases where the LR method does not provided a unique solutions.

The Bayesian approach is increasingly favored, by the entire community. Contrary to the LR method that is data-driven, the Bayesian approach uses a model for reference (prior) and thus can be applied also to small samples and areas. This is a strength of the method but the fact that it assumes the "model distribution" might be not representative of the reality is a frequent criticism. These criticisms are legitimate in general but in the specific case of finding the counterpart to X-ray detected sources they are somewhat outdated. In fact, deep *Chandra* and *XMM* surveys are so advanced/extended that reliable models of magnitude distribution of the counterparts to sources detected up to a desired depth, can now be constructed from data in literature. Another virtue of the Bayesian approach is that many priors can be adopted, each independent from the next. So we can adopt a Bayesian form for the probability of a sources to be the right counterpart based on its position, its magnitude, color etc.

At the basis of many Bayesian cross-matching algorithms is the formalism introduced by Budavári & Szalay (2008)[15], which allows to work simultaneously with multiple catalogues and provided the Bayesian factor for the astrometric measures. This Bayes factor from the astrometry is

---

[15] However, the work does not correctly account for the sources that for physical reasons (e.g. due to the shape of the SED, redshift value) are missed in some of the catalogues. This has been pointed out by many authors (e.g. Roseboom et al. 2009; Pineau et al. 2011)

then combined with one (or more) related to physical properties. It is the case, for example of Roseboom et al. (2009) who search the right counterparts to sub-millimeter sources by computing the photometric redshift and SED fitting of each source within a certain radius circle.

Independently from the method adopted, an additional difficulty rises when the goal is to find the counterpart to large X-ray surveys, over hundreds of square degrees (e.g., eROSITA: Merloni et al. 2012). In this case, the multi-wavelength catalogues from where to draw the correct identification will not be homogeneous covering the field, but rather a patchwork of different surveys/depths, thus effecting the actual magnitude distribution of the field sources and thus the determination of the real counterpart.

In view of these new challenges, we designed Nway, an algorithm based on two-steps Bayesian approach. In the following we provide the complete description of the code and its application to test cases in COSMOS. The code is here released, together with a detailed manual and a set of date for testing purposes.

APPENDIX B: MATCHING METHODOLOGY

This section lays out in detail the computation Nway performs. Further details and clear explanations on the use of the Nway are presented in the manual and tutorial of the code, distributed via Github at https://github.com/JohannesBuchner/nway.

The features of Nway include:

(i) Matching of N catalogues simultaneously.

(ii) Computation of all combinatorially possible matches.

(iii) Consideration of partial matches across catalogues, i.e. the absence of counterparts in some catalogues.

(iv) Taking into account the positional uncertainties and the source number densities, computation of the probability of each possible match.

(v) Computation of the probability that there is no match.

(vi) Incorporating magnitude, color or other information about the sources of interest, refining the match probabilities.

This is done in several steps:

(i) Finding combinatorially all possible matches. See Section B1.

(ii) Computing each match probability from number densities, separation distances and positional errors alone, taking into account the chance of a random alignment. See Section B2.

(iii) For each source of the primary catalogue (in the application from this paper: for each the X-ray source), compute (a) the probability that this source does not have a counterpart and (b), assuming this source has a counterpart, compute the relative probability for each possible match. See Section B3.

(iv) Refining the probabilities by additional prior information. See Section B4.

In Nway, only the first catalogue (*primary catalogue*) has a special role. For every entry in this catalogue, matches are

Input:

Primary Catalogue
x1
x2
...

2nd Catalogue
b1
b2
...

3rd Catalogue
c1
c2
...

Output:

Primary Cat. Entry	2nd Cat. Entry	3rd Cat. Entry	Proba-bility	
x1	b1	c1	...	
x1	b1	c2	...	
x1	b1	(none)	...	
x1	b2	c1	...	
x1	b2	c2	...	source x1
x1	b2	(none)	...	
x1	(none)	c1	...	
x1	(none)	c2	...	
x1	(none)	(none)	...	
x2	...	...	...	source x2

Figure B1. All possible combinations of matches from the input catalogues are combined into the output catalogue. Each such match has a computed probability, either based on positions and number densities or additionally refined after the adoption of one or more priors. The matches are grouped by the primary catalogue entries (here: x1, x2).

sought in the other catalogues. The entries in the primary catalogue must come with an ID. All catalogues must contain RA, DEC, positional error information, the size of the area of sky covered by the catalogue. The latter information is used to compute the probability of a chance alignment.

B1 Computing all possible matches

First, possible associations are found. Figure B1 shows that all possible associations between the input catalogues are considered when building the output catalogue. For this, a hashing procedure puts each object into HEALPix bins (Górski et al. 2005). The bin width w is chosen so that an association of distance w is improbable, i.e. much larger than the largest positional error. An object with coordinates ϕ, θ is placed in the bin corresponding to its coordinate, but also into its neighboring bins to avoid boundary effects. This is done for each catalogue separately. Then, in each bin, the Cartesian product across catalogues (every possible combination of sources) is computed. All associations are collected across the bins and filtered to be unique. The hashing procedure adds very low effort $O(\sum_{i=1}^{k} N_i)$ while the Cartesian product is reduced drastically to $O(N_{\text{bins}} \cdot \prod_{i=1}^{k} \frac{N_i}{N_{bins}})$, from a naive approach complexity of $O(\prod_{i=1}^{k} N_i)$ All primary objects that have no associations past this step have $P("any real association"|D) = 0$.

A problem arises when the secondary catalogues have depths or resolution such that some of the sources appear only in some of the catalogues . So we need to consider also pairing that do not include a source from the primary catalog. The computation becomes infeasible very quickly as the number of catalogues reaches four or more, as demonstrated in Pineau et al. (2017).

Nway first considers as an initial list all possibilities

which have the primary catalogue source in an association. As shown above, this includes associations where some catalogues do not participate. The remaining sources are considered independent. Secondly, associations across the unused catalogues are considered for each case. To do this with low computational complexity, the additional associations considered are those in the initial list, but with the primary catalogue source removed. For instance, for the case of primary source x1 with the other sources independent, x1-(none)-(none), the additional associations to consider are x1-b1-c1, x1-b1-c2, x1-b2-c1, x1-b2-c2, i.e. with the primary source removed, b1-c1, b1-c2, b2-c1, b2-c2. The highest distance-based posterior of these additional associations is factored into the distance-based posterior of the association with the primary source. In practice, this solves the problem of tight unrelated associations (e.g. b2-c1), which, if not considered otherwise, would unduly favor an association which includes them (e.g. x1-b1-c1). If five or more catalogues are matched, not only one but two additional simultaneous association might need to be considered. The impact of our approximation then depends on the application. Our choice of using the highest posterior over all unrelated associations is expected to handle such many-catalogue applications well. If however several groups of similar nature (e.g., a X-ray catalogue, two radio catalogues and three optical catalogues) are to be matched, proceeding hierarchically may give better results (e.g. first match the optical catalogues together). However, more testing is needed in this area.

B2   Distance-based matching

The second step is the computation of association probabilities using the angular distances between counterparts. In the last step (Section B3), for each source in the primary catalogue these probabilities from the various possible matches are combined. In the end this gives the probability that this source does not have a counterpart and, assuming this source has a counterpart, compute the relative probability for each possible match. At this step however we first compute the probability for a particular association (e.g. x1-b1-c1, or x1-(none)-c2) to be actually the same object versus a chance alignment of unrelated objects.

The probability of a given association is computed by comparing the probability of a random chance alignment of unrelated objects (prior) to the likelihood that the sources from the various catalogues are in fact the same object. The prior is evaluated from the density of each catalogue and their effective coverage. Varying depths between the catalogues and different coverage can further reduce the fraction of expected matches, which can be adjusted for with a user-supplied incompleteness factor. The posterior for each association based on the distances only is calculated (output column dist_post). The mathematical details of this computation be found in Section B5. This probability can be modified by additional information (see Section B4).

B3   Grouping, Flagging and Filtering

In the final step, associations are grouped by the source from the primary catalogue (in our example, the X-ray catalogue). The posterior probabilities that this source has any real association and the relative probability for each match are computed (output columns p_any and p_i respectively). Section B5 details this computation. To remove low-probability associations from the output catalogue, the user parameter --min-prob can be used to specify a threshold. The best match is indicated with match_flag=1 for each primary catalogue entry. Secondary, almost as good solutions are marked with match_flag=2[16]. By default associations are flagged with match_flag=2 as soon as p_i$_{match\_flag=1}$/p_i$_{match\_flag=2}$ > 0.5, but the use can change the threshold with the parameter --acceptable-prob. All other associations are marked with match_flag=0.

In the output catalogue the last three columns (p_any, p_i, match_flag) allow the user to identify sources with one solution, possible secondary solutions, and to build final catalogues.

B4   Matching with additional prior information

For many classes of sources, the Spectral Energy Distribution (SED) provides additional hints which associations are likely real. For instance, the WISE color distribution is different for X-ray sources than for other objects (demonstration in Section 4.1). A powerful feature of Nway is to take advantage of this additional information to improve the matching. In particular Nway allows:

(i) Multiple priors to be used from any of the input catalogues.

(ii) Arbitrary quantities can be used. Providing priors is not limited to magnitude distributions, one can use any other discriminating information (e.g. colors, morphology, variability, etc.).

(iii) It is possible to input pre-constructed information, or compute the distributions from the catalogues themselves based on secure distance-only matches (see Section B6.1).

Section B6 has the mathematical details and a comparison to the Likelihood Ratio method (Sutherland & Saunders 1992)

B5   Probability for a individual association

Let us consider the problem of finding counterparts to a primary catalogue ($i = 1$), in our example for the X-ray source position catalogue. Let each N_i denote the number of entries for the catalogues used, and $\nu_i = N_i/\Omega_i$ denote their respective source surface density on the sky.

If a counterpart is required to exist in each of the k catalogues, there are $\prod_{i=1}^{k} N_i$ possible associations. If we assume that a counterpart might be missing in each of the matching catalogues, there are $N_1 \cdot \prod_{i=2}^{k}(N_i + 1)$ possible associations. This minor modification, negligible for $N_i \gg 1$, is ignored in the following for simplicity, but handled in the code.

If each catalogue covers the same area with some respective, homogeneous source density ν_i, the probability of a chance alignment on the sky of k physically unrelated objects can then be written (Budavári & Szalay 2008, eq. 25)

---

[16] While there can be only one source from the secondary catalogues with match_flag=1 per each source of the primary catalog, there can be many that are flagged match_flag=2

as

$$P(H) = N_1 / \prod_{i=1}^{k} N_i = 1 / \prod_{i=2}^{k} N_i = 1 / \prod_{i=2}^{k} \nu_i \Omega_i. \qquad (B1)$$

Thus $P(H)$ is the prior probability of an association. The posterior should strongly exceed this prior probability, to avoid false positives.

To account for non-uniform coverage, $P(H)$ is modified by a "prior completeness factor" c, which gives the expected fraction of sources with reliable counterpart (due to only partial coverage of the matching catalogues $\Omega_{i>1} \neq \Omega_1$, depth of the catalogues and/or systematic errors in the coordinates). Our prior can thus be written as

$$P(H) = c / \prod_{i=2}^{k} \nu_i \Omega_1. \qquad (B2)$$

Bayes theorem connects the prior probability $P(H)$ to the posterior probability $P(H|D)$, by incorporating information gained from the observation data D via

$$P(H|D) \propto P(H) \times P(D|H). \qquad (B3)$$

We now extend the approach of Budavári & Szalay (2008), to allow matches where some catalogues do not participate in a match. Comparing A12 and A14 in Budavári & Szalay (2008), assuming that positions lie on the celestial sphere and adopting the expansions developed in their Appendix B, we can write down likelihoods. For a counterpart across k catalogues, we obtain:

$$P(D|H) = 2^{k-1} \frac{\prod \sigma_i^{-2}}{\sum \sigma_i^{-2}} \exp \left\{ -\frac{\sum_{i<j} \phi_{ij} \sigma_j^{-2} \sigma_i^{-2}}{2 \sum \sigma_i^{-2}} \right\} \qquad (B4)$$

The likelihood for the hypothesis where some catalogues do not participate in the association has the appropriate terms in the products and sums removed. Therefore, the likelihood is unity for the hypothesis that there is no counterpart in any of the catalogues.

In comparison to our method, the method of Budavári & Szalay (2008) only compares two hypotheses for a association: either all sources belong to the same object (H_1), or they are coincidentally aligned (H_0). In this computation each hypothesis test is run in isolation, and relative match probabilities for a given source are not considered. For completeness, we also compute the posterior of this simpler model comparison:

$$\frac{P(H_1|D)}{P(H_0|D)} \quad \propto \quad \frac{P(H_1)}{P(H_0)} \times \frac{P(D|H_1)}{P(D|H_0)} \qquad (B5)$$

$$B \quad = \quad \frac{P(D|H_1)}{P(D|H_0)} \qquad (B6)$$

$$P(H_1|D) \quad = \quad \left[1 + \frac{1 - P(H_1)}{B \cdot P(H_1)} \right]^{-1} \qquad (B7)$$

The output column `dist_bayesfactor` stores $\log B$, while the output column `dist_post` is the result of equation B7. The output column `p_single` is the same as `dist_post`, but modified if any additional information is specified (see Section B6). As mentioned several times in the literature, the Budavári & Szalay (2008) approach does not include sources absent in some of the catalogues, while the formulae

we develop below incorporate absent sources. This is similar in spirit to Pineau et al. (2017), although the statistical approach is different. We now go further and develop counterpart probabilities.

The first step in catalogue inference is whether the source has any counterpart (`p_any`).The posterior probabilities $P(H|D)$ are computed using Bayes theorem (eq. B3) with the likelihood (eq. B4) and prior (eq. B2) appropriately adopted for the number of catalogues the particular association draws from. For each entry in the primary catalogue, the posteriors of all possible associations are normalized to unity, and $P(H_0|D)$, the posterior probability of the no-counterpart hypothesis, i.e., no catalogue participates, computed. From this we compute:

$$\texttt{p\_any} = 1 - P(H_0|D) / \sum_i P(H_i|D) \qquad (B8)$$

If `p_any` is low, this indicates that there is little evidence for any of the considered, combinatorially possible associations, except for the no-association case. The output column `p_any` is the result of equation B8.

If `p_any` ≈ 1, there is strong evidence for at least one of the associations to another catalogue. To compute the relative posterior probabilities of the options, we re-normalize with the no-counterpart hypothesis, H_0, excluded:

$$\texttt{p\_i} = P(H_i|D) / \sum_{i>0} P(H_i|D) \qquad (B9)$$

If a particular association has a high p_i, there is strong evidence that it is the true one, out of all present options. The output column `p_i` is the result of equation B9.

A "very secure" counterpart could be defined by the requirement `p_any`>95% and `p_i`>95%, for example. However, it is useful to run simulations to understand the rate of false positives. Typically, much lower thresholds are acceptable, with the threshold (dictated by the scientific applications) being a compromise between purity and completeness of the sample.

B6 Magnitudes, Colors and other additional information

Specific classes of astronomical objects show distinct distribution on color, magnitude or other parameters, compared to the field population distributions. This can be exploited for finding the correct counterparts. Previous works (e.g. Ciliegi et al. 2003, 2005; Brusa et al. 2005, 2007) have modified the likelihood ratio coming from the angular distance $f(r)$ information (likelihood ratio method, Sutherland & Saunders 1992) by a factor:

$$LR = \frac{q(m)}{n(m)} \times f(r) \qquad (B10)$$

Here, $q(m)$ and $n(m)$ are associated with the magnitude distributions of source (e.g. X-ray sources) and background objects respectively, but additionally contain sky density contributions.

This idea can be put on solid footing within the Bayesian framework. Here, two likelihoods are combined,

by simply considering two independent observations, namely one for the positions, D_ϕ, and one for the magnitudes D_m. The likelihood thus becomes

$$P(D|H) = P(D_\phi|H) \times P(D_m|H) \quad \text{(B11)}$$

$$= P(D_\phi|H) \times \frac{\bar{q}(m)}{\bar{n}(m)}, \quad \text{(B12)}$$

with $\bar{q}(m)$ and $\bar{n}(m)$ being the probability that a target (e.g. X-ray) source or a generic source in the field has magnitude m, respectively.

Nway stores the modifying factor, $P(D_m|H)$, in `bias_*` output columns, one for each column giving a magnitude, color, or other distribution. This modifying factor is however renormalized so that $P(D_m|H) = \frac{\bar{q}(m)}{\bar{n}(m)} / \int \frac{\bar{q}(m')}{\bar{n}(m')} \bar{n}(m') dm'$, which makes $P(D|H) = P(D_\phi|H)$ when m is unknown. In that case, m is marginalized over its distribution in the general population, i.e. $\int P(D_m|H) \bar{n}(m') dm$. This has the benefit that when m is unknown, the modifying factor is unity and the probabilities remain unmodified.

For completeness, we mention the fully generalized case. This is attained when an arbitrary number of photometry bands are considered, each consisting of a magnitude measurement m and measurement uncertainty σ_m:

$$P(D_m|H) = \prod \frac{\int_m \bar{q}(m)\, p(m|D_m)\, dm}{\int_m \bar{n}(m)\, p(m|D_m)\, dm} \quad \text{(B13)}$$

Here, $p(m|D_m)$ would refer to a Gaussian error distribution with mean m and standard deviation σ_m. This is convolved with the distribution properties. Alternatively, $p(m|D_m)$ can also consider upper limits. However, such options are not yet implemented in Nway. Instead, we recommend removing magnitude values with large uncertainties (setting them to -99).

B6.1   Auto-calibration

The probability distributions $\bar{n}(m)$ and $\bar{q}(m)$ can be taken from other observations by computing the normalized magnitude[17] histograms of the overall population and the target sub-population (e.g. X-ray sources). In Nway, the distributions $\bar{q}(m)$ and $\bar{n}(m)$ can be provided as a ASCII table, with the columns describing the bin edges, the frequency of the target population (in our example, X-ray sources) and the frequency of the field population (sources that are not X-ray sources, at the depth of the catalogue).

Under certain approximations and assumptions, these histograms can also be computed during the catalogue matching procedure used for the weighting on the fly and saved for future further use. For example, one could perform the distance-based matching procedure laid out above, and compute a magnitude histogram of the secure counterparts as an approximation for $\bar{q}(m)$ and a histogram of ruled out counterparts for $\bar{n}(m)$. While the weights $\bar{q}(m)/\bar{n}(m)$ may strongly influence the probabilities of the associations for

a single object, the bulk of the associations will be dominated by distance-weighting. One may thus assume that the $\bar{q}(m)$ and $\bar{n}(m)$ are computed with and without applying the magnitude weighting are the same, which is true in practice. When differences are noticed, they will only strengthen $\bar{q}(m)$, and the procedure may be iterated.

In Nway auto mode, the histogram $\bar{q}(m)$ is constructed using sources with `dist_post>0.9` (safe matches), and $\bar{n}(m)$ with `dist_post<0.01` (safe non-matches). When these "self constructed priors" are used, the breaks of the histogram bins are computed adaptively based on the empirical cumulative distribution found. Because the histogram bins are usually larger than the magnitude measurement uncertainty, the latter is currently not considered. The adaptive binning creates bin edges based on the number of objects, and is thus independent of the chosen scale (magnitudes, flux). Thus the method is not limited to magnitudes, but can be used for virtually any other known object property (colors, morphology, variability, etc.), as demonstrated in the main body of this paper.

APPENDIX C: TESTING Nway ON COSMOS

The COSMOS (Scoville et al. 2007) field offers the ideal test bench as it covers a relatively large area and has homogeneous and deep observations in many bands. In particular, the field has been observed with *XMM-Newton* (Hasinger et al. 2007; Cappelluti et al. 2007), and its reliable association to the I-band CFHT/Megacam catalogueMcCracken et al. (2007) via LR is presented in Brusa et al. (2007). Successively, Brusa et al. (2010) improved on the first associations using also the near- infrared (McCracken et al. 2010) and the mid-infrared (Sanders et al. 2007; Ilbert et al. 2010) catalogues. Each catalogue were used independently and the counterparts chosen via LR and visually inspected.

More recently, for the same area, deeper and homogeneous observations from *Chandra* became available (Elvis et al. 2009; Civano et al. 2012, 2016; Marchesi et al. 2016) so that the XMM-COSMOS associations have been successively validated/changed on the basis of the smaller positional uncertainties of the *Chandra* X-ray data[18] ($\sim 0.5''$ vs. $\sim 2''$ for XMM, averaging over the entire FOV).

In the following two sections we describe the successful application of Nway to the XMM-COSMOS field, first using only one optical catalogue. We then repeated the association using simultaneously the optical and IRAC catalogues. We show how the associations and the key Nway parameters `p_i` and `p_any` change in the two applications. Both the optical and IRAC catalogues are the original used by Brusa et al. (2010). They are released with Nway and described in the manual so that a curious reader can practice with the code.

C1   Nway Success rate

The XMM-COSMOS catalogue of multi-wavelength counterparts presented in Brusa et al. (2010) included 1822 sources, 1797 of which are isolated sources[19]. We focus here

---

[17] We make the examples using magnitudes, but everything will work the same using any other parameter like colors, morphology, variability etc.

[18] The user should refer to Marchesi et al. (2016) for details about the comparison between XMM-/*Chandra*- COSMOS detections.
[19] i.e. 25 sources correspond to two or more ıChandra detections

on the 1281(128) *XMM*-COSMOS isolated sources with the original confirmed(changed) association after using *Chandra* data.

We extracted from the catalogue of Brusa et al. (2010) the identification number, the X-ray coordinates and corresponding positional errors of the 1409 (1281+128) isolated sources. The mean positional error of the sample is $1.8''$ with a minimum value of $0.1''$ to a max of $7.33''$. Similarly, we extracted from the optical (McCracken et al. 2007) and IRAC (Sanders et al. 2007; Ilbert et al. 2010) catalogues the identification numbers, the coordinates and the magnitude in the optical and $3.6\ \mu m$ bands. We assumed, as in Brusa et al. (2007) a constant positional error of $0.1''$ and $0.5''$ for the two catalogues , respectively.

First, we run Nway between the *XMM* and optical catalogues in mode "auto" (see §B6.1). Although we know that for this sample the actual counterparts are within $8''$ from the X-ray positions, we searched for a counterpart within a radius of $20''$ in order to avoid any bias in the result. In the 96% (1231/1281) of the cases Nway assigned the same counterpart[20] as in Brusa et al. (2007). In addition, of the 128 sources for which the counterpart has changed thanks to the higher resolution of *Chandra*, Nway recovered correctly (and independently) 55 of them (i.e. 43%).

In the second test, we run Nway again in mode "auto", but this time pairing simultaneously the *XMM* catalogue to the optical and IRAC catalogues. Intuitively, increasing the number of priors the number of correct associations should increase. At the same time, the number of matches due to chance association should decrease. In particular, a second prior will reinforce the probability that a source is the correct counterpart, or, provide an alternative, better counterpart. In fact in this second application we recovered correctly 1250/1281 (97.6%) sources. Of the 128 sources that change counterpart after *Chandra* observations, we recovered correctly 65 (50.8%) of them, without any additional information. The new sources were either very faint or completely missed in optical catalog.

C2 Nway parameters behaviors

As discussed when describing the code, Nway provides informative quantities `p_any` and `p_i` that can help in assessing the reliability of an association. The first parameter indicates what is the probability that an X-ray sources has at least a reliable counterpart among the possible associations, behaving as the prior. Low `p_any` may indicate that either the prior is not able to disentangle between possible counterparts, or that none of the possible counterparts behave as the prior. The second parameter, `p_i` indicates what is the probability for a given source to be the correct counterpart among the possible associations to an X-ray source.

In Figure C2 we show `p_i` versus `p_any` for the optical prior (OPT, top-left panel) and for the optical+IRAC prior (OPT+MIR, bottom-left panel.). In Addition we show the respective cumulative distribution of `p_any` (right panels). Additionally, we plot in grey the same parameters as before computed for random associations. This was obtained

by applying Nway to the same catalogues , but after randomizing the position of the X-ray sources by shifting by $1'$ their declination.

From the top plots we can see that the distribution of `p_any` for the random position, concentrate at low values of `p_any` while the `p_any` peak at high values. For example `p_any`$_{real}$ > 0.6 for 80% of the counterpart to real X-ray sources while only 0.09% of the counterparts to randomized X-ray sources have such high `p_any`[21].

The term `p_i` is the combination of two terms, one related to the pure positional match and one related to the prior. If the number density of sources in the optical catalogue is high, there will be always a possible counterpart due to chance association, for the randomized X-ray sources. For this reason, more than 40% of the possible counterparts to the randomized X-ray source have `p_i`>0.8. Only coupling `p_i` with `p_any` we can find out the actual nature of the counterpart.

The situation changes noticeably on the bottom panels of Figure C2, where not one but two priors (one in Optical and one in mid-infrared) are simultaneously considered. Here, the distribution of `p_i` and `p_any` is similar to the previous case, while for the counterpart to actual X-ray sources, both parameters peak at high values. Again, worth of note is the fact that 99.9% of the counterparts were correctly identified already with a single prior. The additional prior just increased `p_i` indicating how the real counterparts clearly stand up from the field distribution. Intuitively, adding a third prior would reduce even strongly the possibility that a counterpart is selected due to chance association.

Finally, an important point to stress is that while the original work on the *XMM* and *Chandra* associations took months and an additional visual inspection was necessary, the reliable results presented here for Nway where obtained in less than 5 minutes with a single 2700MHz CPU without any filtering or inspection.

REFERENCES

Altmann M., Roeser S., Demleitner M., Bastian U., Schilbach E., 2017, A&A, 600, L4
Arenou F., et al., 2017, A&A, 599, A50
Armstrong T., Brown A. M., Chadwick P. M., Nolan S. J., 2015, MNRAS, 452, 3159
Assef R. J., et al., 2013, ApJ, 772, 26
Baumgartner W. H., Tueller J., Markwardt C. B., Skinner G. K., Barthelmy S., Mushotzky R. F., Evans P. A., Gehrels N., 2013, ApJS, 207, 19
Boller T., Freyberg M. J., Trümper J., Haberl F., Voges W., Nandra K., 2016, A&A, 588, A103
Bovy J., et al., 2011, preprint, (arXiv:1105.3975)
Brusa M., et al., 2005, A&A, 432, 69
Brusa M., et al., 2007, ApJS, 172, 353
Brusa M., et al., 2010, ApJ, 716, 348
Budavári T., Szalay A. S., 2008, ApJ, 679, 301
Budavári T., Szalay A. S., Loredo T. J., 2017, ApJ, 838, 52
Cappelluti N., et al., 2007, ApJS, 172, 341
Chambers K. C., et al., 2016, preprint, (arXiv:1612.05560)

---

[20] For this test we consider as counterpart the source with the highest `p_any``p_i` within each circle

[21] Note that we can not exclude that these 0.09% sources are the counterpart to real X-ray sources that are fainter that the depth of our survey
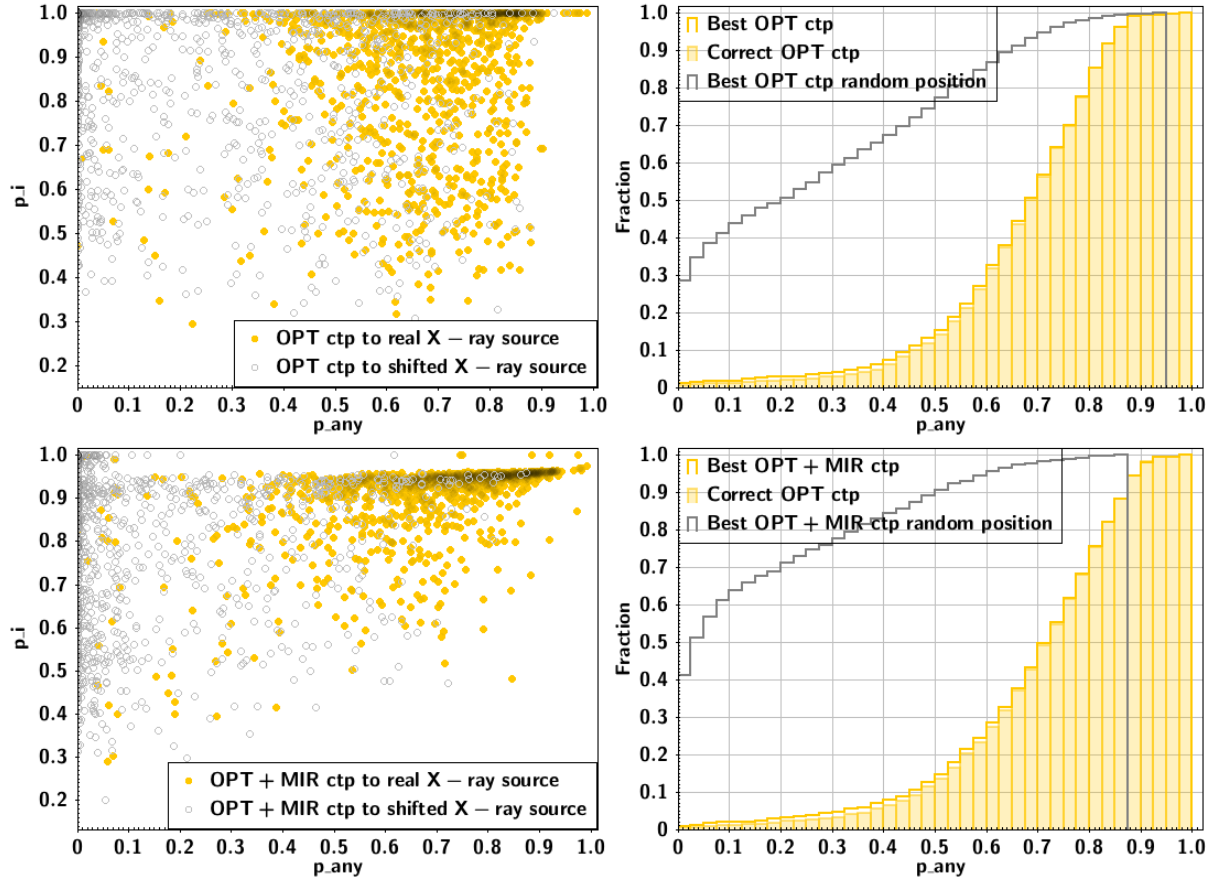
Figure C1. Top left: `p_i` vs. `p_any` distribution for the correct counterparts to the *XMM*-COSMOS sources (yellow) and for the candidate counterpart to the same sources after randomizing their position (grey), using only the optical catalog.**Top right:** Cumulative distribution of `p_any` for the actual sample of correct counterparts (solid yellow) and for the counterparts to the randomized X-ray sources (solid grey). The dashed yellow line represent the distribution, including also the 26 sources for which Nway fails in identifying the correct counterparts. These sources have all `p_any` below 0.5 (after that value the two yellow curves coincide).**Bottom left:** and **Bottom right:** As above, but this time using simultaneously a prior in Optical and one in mid-infrared.

Ciliegi P., Zamorani G., Hasinger G., Lehmann I., Szokoly G., Wilson G., 2003, A&A, 398, 901

Ciliegi P., et al., 2005, A&A, 441, 879

Civano F., et al., 2012, ApJS, 201, 30

Civano F., et al., 2016, ApJ, 819, 62

Condon J. J., Cotton W. D., Greisen E. W., Yin Q. F., Perley R. A., Taylor G. B., Broderick J. J., 1998, AJ, 115, 1693

Cutri R. M., et al., 2013, Technical report, Explanatory Supplement to the AllWISE Data Release Products

D'Abrusco R., Massaro F., Paggi A., Masetti N., Tosti G., Giroletti M., Smith H. A., 2013, ApJS, 206, 12

De Breuck C., van Breugel W., Röttgering H., Carilli C., 2002, in Green R. F., Khachikian E. Y., Sanders D. B., eds, Astronomical Society of the Pacific Conference Series Vol. 284, IAU Colloq. 184: AGN Surveys. p. 275 (arXiv:astro-ph/0111254)

Dwelly T., et al., 2017, preprint, (arXiv:1704.01796)

Elvis M., et al., 2009, ApJS, 184, 158

Fabricius C., et al., 2016, A&A, 595, A3

Fotopoulou S., et al., 2012, ApJS, 198, 1

Fotopoulou S., et al., 2016, A&A, 592, A5

Georgakakis A., Nandra K., 2011, MNRAS, 414, 992

Georgakakis A., et al., 2017, preprint, (arXiv:1704.08296)

Gioia I. M., Maccacaro T., Schild R. E., Wolter A., Stocke J. T., Morris S. L., Danziger I. J., 1987, in Khachikian E. E., Fricke K. J., Melnick J., eds, IAU Symposium Vol. 121, Observational Evidence of Activity in Galaxies. p. 329

Górski K. M., Hivon E., Banday A. J., Wandelt B. D., Hansen F. K., Reinecke M., Bartelmann M., 2005, ApJ, 622, 759

Gressler W., et al., 2014, in Ground-based and Airborne Telescopes V. p. 91451A, doi:10.1117/12.2056711

Hasinger G., et al., 2007, ApJS, 172, 29

Hsu L.-T., et al., 2014, preprint, (arXiv:1409.7119)

Ilbert O., et al., 2010, ApJ, 709, 644

Just D. W., Brandt W. N., Shemmer O., Steffen A. T., Schneider D. P., Chartas G., Garmire G. P., 2007, ApJ, 665, 1004

LaMassa S. M., et al., 2015, ApJ, 800, 144

LaMassa S. M., et al., 2016, ApJ, 817, 172

Laigle C., et al., 2016, ApJS, 224, 24

Lang D., Hogg D. W., Schlegel D. J., 2016, AJ, 151, 36

Luo B., et al., 2008, ApJS, 179, 19

Luo B., et al., 2010, ApJS, 187, 560

Luo B., et al., 2017, ApJS, 228, 2

Lusso E., et al., 2010, A&A, 512, A34

Maccacaro T., Gioia I. M., Wolter A., Zamorani G., Stocke J. T., 1988, ApJ, 326, 680

Mahony E. K., Croom S. M., Boyle B. J., Edge A. C., Mauch T., Sadler E. M., 2010, MNRAS, 401, 1151

Mainzer A., et al., 2011, ApJ, 731, 53

Mainzer A., et al., 2014, ApJ, 792, 30

Marchesi S., et al., 2016, ApJ, 817, 34

McCracken H. J., et al., 2007, ApJS, 172, 314

McCracken H. J., et al., 2010, ApJ, 708, 202

Meisner A. M., Lang D., Schlegel D. J., 2016, in American Astronomical Society Meeting Abstracts. p. 140.03
Meisner A. M., Lang D., Schlegel D. J., 2017, preprint, (arXiv:1705.06746)
Merloni A., et al., 2012, preprint, (arXiv:1209.3114)
Merloni A., et al., 2015, MNRAS, 452, 69
Myers A. D., et al., 2015, ApJS, 221, 27
Nandra K., et al., 2015, ApJS, 220, 10
Nikutta R., Hunt-Walker N., Nenkova M., Ivezić Ž., Elitzur M., 2014, MNRAS, 442, 3361
Norris R. P., et al., 2011, Publ. Astron. Soc. Australia, 28, 215
Oosterloo T., Verheijen M., van Cappellen W., 2010, in ISKAF2010 Science Meeting. p. 43 (arXiv:1007.5141)
Palanque-Delabrouille N., et al., 2016, A&A, 587, A41
Pâris I., et al., 2017, A&A, 597, A79
Pierre M., et al., 2017, Astronomische Nachrichten, 338, 334
Pineau F.-X., Motch C., Carrera F., Della Ceca R., Derrière S., Michel L., Schwope A., Watson M. G., 2011, A&A, 527, A126
Pineau F.-X., et al., 2017, A&A, 597, A89
Rau A., et al., 2009, PASP, 121, 1334
Roeser S., Demleitner M., Schilbach E., 2010, AJ, 139, 2440
Roseboom I. G., Oliver S., Parkinson D., Vaccari M., 2009, MNRAS, 400, 1062
Rosen S. R., et al., 2016, A&A, 590, A1
Runnoe J. C., et al., 2016, MNRAS, 455, 1691
Rutledge R. E., Brunner R. J., Prince T. A., Lonsdale C., 2000, ApJS, 131, 335
Salvato M., et al., 2011, ApJ, 742, 61
Sanders D. B., et al., 2007, ApJS, 172, 86
Schwope A., et al., 2000, Astronomische Nachrichten, 321, 1
Scoville N., et al., 2007, ApJS, 172, 38
Steffen A. T., Strateva I., Brandt W. N., Alexander D. M., Koekemoer A. M., Lehmer B. D., Schneider D. P., Vignali C., 2006, AJ, 131, 2826
Stern D., et al., 2012, ApJ, 753, 30
Strateva I. V., Brandt W. N., Schneider D. P., Vanden Berk D. G., Vignali C., 2005, AJ, 130, 387
Sutherland W., Saunders W., 1992, MNRAS, 259, 413
Taylor M. B., 2005, in Shopbell P., Britton M., Ebert R., eds, Astronomical Society of the Pacific Conference Series Vol. 347, Astronomical Data Analysis Software and Systems XIV. p. 29
Taylor M. B., 2006, in Gabriel C., Arviset C., Ponz D., Enrique S., eds, Astronomical Society of the Pacific Conference Series Vol. 351, Astronomical Data Analysis Software and Systems XV. p. 666
Truemper J., 1982, Advances in Space Research, 2, 241
Tsai C.-W., et al., 2013, ApJ, 779, 41
Vignali C., Brandt W. N., Schneider D. P., 2003, AJ, 125, 433
Voges W., et al., 1999, A&A, 349, 389
Voges W., et al., 2000, VizieR Online Data Catalog, 9029, 0
Wood K. S., et al., 1984, ApJS, 56, 507
Wright N. J., Drake J. J., Civano F., 2010, ApJ, 725, 480
Xue Y. Q., et al., 2011, ApJS, 195, 10
Young M., Elvis M., Risaliti G., 2010, ApJ, 708, 1388
van Haarlem M. P., et al., 2013, A&A, 556, A2

This paper has been typeset from a TEX/LATEX file prepared by the author.